Politecnico di Torino

Corso di laurea magistrale in Ingegneria dei Materiali

Optimization of shear mode solidly mounted resonators based on fully-dielectric acoustic reflectors for biosensing applications

Master thesis

Martino Ramotti

Supervisor:

Dr. Candido Pirri (Politecnico di Torino)

Dr. Teona Mirea (Universidad Politecnica de Madrid)

Summary

Electroacoustic biosensors are widely studied nowadays as they can provide a complete and cheap solution for the real time detection of virus, or different diseases, in a very small liquid sample (e.g. blood, urine, saliva). One of these electroacoustic sensors are based on Solidly Mounted Resonators (SMRs). These devices have proven their potential as biosensors but never been optimized from their acoustic reflector point of view. Most of the optimizations were focused on the deposition of tilted piezoelectric materials to excite an acoustic shear mode, the one needed to operate in liquid.

The objective of this thesis was to perform a full optimization of the SMR technology for its use as biosensor. The optimization included the design, simulation, and fabrication of the device and its final test in a real biosensing experiment. Unfortunately, the Covid-19 emergency brought some difficulty and the work had to be re-organized in a different way. The work was then focused more on a simulation approach as we could fabricate just few devices. The biosensing verification was finally not performed, however the few devices fabricated could prove the theoretical simulations.

The main focus of the thesis was the optimization of the acoustic reflector for the shear mode operation, as this acoustic mode doesn't couple with liquids and allows the resonator to work in a liquid medium. Two different approaches were used, and the designed acoustic reflector performances were simulated with the 1D Mason's model and with a 2D FEM analysis. The same reflectors were also fabricated, and besides the emergency, reliable measurements were obtained.

The results of the simulations suggest that the optimized designs significantly improve the performances of the resonators in terms of reflectance of the mirrors and resonator Q factor values. Moreover, the experimental results verify the theoretical predictions.

Contents

1. Introduction and objectives

1.1 Introduction

Electroacoustic (EA) resonators are widely known for their use as RF filters in the telecommunication industry [1]. They can work in different frequency ranges depending on the materials and structures used. EA devices based on bulk single crystal materials work up to the MHz ranges, while EA devices based on thin films (thicknesses below 3 µm) can work in the GHz ranges [2] [3]. These last have become crucial for the next 5G generation.

Besides their established use as RF filters, during the last decades EA devices have been widely studied as different types of high-resolution sensors: chemical, physical or biological [4] [5]. Their ability to detect mass attached to their surface (i.e. gravimetric) and their new working frequencies in the GHz range have provided these EA resonators with detection limits of few picograms [6] [7].

One of their most studied application is as biosensors. These sensors can detect biological particles as proteins, virus, bacteria etc, in different fluids like blood, urine or saliva, among others. The most typical biosensors nowadays are either electrochemical or optical ones. However, electroacoustic sensors present several advantages that place them as potential competitors:

- High resolution and low detection limits.
- Low cost production as their fabrication is based on well-established technologies from the Telcom industry.
- Dimensions in the micrometric range.
- Easy array integration for multiple detection.
- Integration with Si-based chips, which allows having on the same chip the sensor and the electronics, thus reducing the costs.

One specific type of EA device widely studied as biosensor is the Solidly Mounted Resonator (SMR) working in the acoustic shear mode [8] [9]. This mode is not degraded when the device surface is contacted by liquid. Many studies have been focused on optimizing the generation of the shear waves in the resonator [10] [11]. However, the device structure optimization that ensures low shear mode losses has not been performed so far. This is important as the performance of the sensor in terms of resolution and noise directly depends on these losses that can degrade the electrical response of the sensor.

In this thesis we will optimize SMR devices to reduce their shear mode losses. We will follow similar techniques to the ones used for their filter counterpart optimization, where the acoustic mode used is the longitudinal one.

1.2 Acoustic wave devices

An acoustic wave device, or EA device, is an electromechanical system able to convert a mechanical stimulus into an electrical signal and vice versa. The core of the EA device is a piezoelectric material, which on one hand generates a mechanical wave when we apply an alternating electrical field (indirect piezoelectric effect), and on the other hand creates an electric field when the elastic recovery of the deformation occurs (direct piezoelectric effect). The presence of two types of energies in the system,

mechanical and electrical, enables the fabrication of resonators in which one interchanges with the other.

A typical classification of the acoustic wave devices is based on their mechanical wave guiding process and distinguishes three main types: Bulk Acoustic Wave devices (BAW), Surface Acoustic Wave devices (SAW) and Acoustic Plate Wave devices (APW). In a BAW device, waves travel unguided in the volume, or bulk, of the material. In a SAW device, waves travel guided along a single surface, while in an APW device waves travel guided in membranes, or plates, confined between both its surfaces by multiple reflections. This classification is illustrated in figure 1. A more detailed overview of the different devices can be found in [12]. In this thesis, a thin film BAW resonator is studied and optimized in view of its application as biosensor.

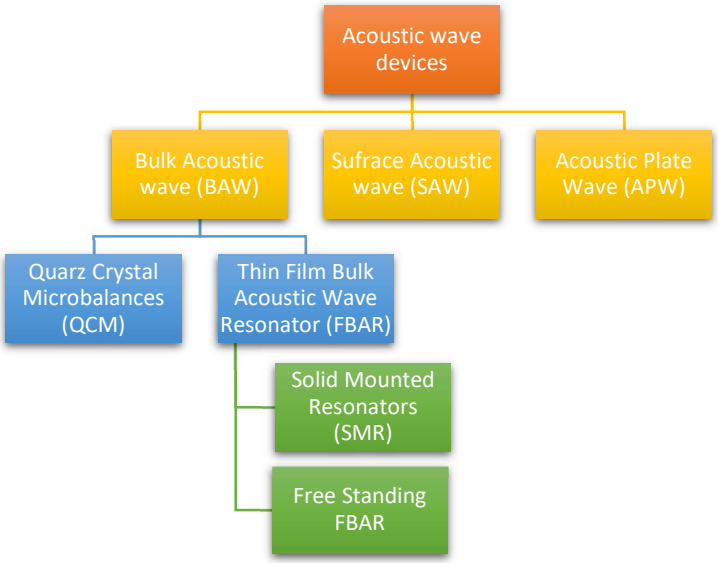

Figure 1: Classification of acoustic wave devices.

1.2.1 Piezoelectricity and AlN

Piezoelectricity was firstly described by Pierre and Jacques Curie in 1880 [13]. They observed that by compressing some crystal it was possible to generate an electric signal, phenomenon today known as direct piezoelectric effect. The inverse piezoelectric effect was mathematically deduced one year later by Gabriel Lippman from thermodinamical considerations and immediately observed by Curie brothers [14], [15].

Linear piezoelectricity arises from the linear coupling of the linear electrical behavior of materials, expressed by Maxwell's equation

$$T = c \cdot S \tag{1}$$

and the linear elastic behavior of materials, expressed by the Hocke's law

$$D = \varepsilon \cdot E \tag{2}$$

where T is the stress, S is the strain, D is the electric displacement, E is the external electric field, ε is permittivity and c is the stiffness.

Both the direct and the inverse piezoelectric effect can be described by the following equations, that are the combination of equation (1) and (2):

$$T = c \cdot S + e \cdot E \quad (3)$$

$$D = \varepsilon \cdot E + e \cdot S \quad (4)$$

Where e is the piezoelectric stress constant, the parameter that connects the mechanical and electrical properties of the material.

The efficiency of a piezoelectric material to convert mechanical energy to electrical, and vice versa, is represented by its intrinsic electromechanical coupling coefficient k^2, which can be expressed as [16]:

$$k^2 = \frac{e^2}{c \cdot \varepsilon} \quad (5)$$

It's important to notice that e, c and ε are elements of a tensor so that the value of k^2 depends on the considered directions.

The crystallographic symmetry of solids has a fundamental role in the appearance of the piezoelectric phenomena, which is related to the occurrence of electric dipoles in the material. These dipoles can be generated either by ions in crystal sites with an asymmetrical surrounding (as in piezoelectric ceramics) or by polar groups in molecules (as in piezoelectric polymers). In all cases, the piezoelectric effect relates to the change of polarization P of the material under the application of a mechanical stress. A detailed description of the microscopic mechanism can be found in [17].

In addition to a good electromechanical coupling coefficient, a good piezoelectric material for EA devices must have large acoustic wave velocity and low acoustic loss and damping. Moreover, for a temperature stable acoustic device, the piezoelectric material must display a low thermal coefficient of frequency (TCF), which is defined as [18]:

$$TCF = \frac{1}{f_0}\frac{df}{dT} \quad (6)$$

The TCF values are normally measured experimentally by recording changes of the frequency values as a function of temperature.

The most typical piezoelectric materials are Quartz, PZT, ZnO and AlN. Among them, PZT has the largest piezoelectric constant and electromechanical coupling coefficient. However, PZT films have disadvantages for biosensing applications such as high acoustic attenuation, low sound wave velocity and difficulty to be fabricated in thin films. Quartz is widely used because of its very low temperature coefficient of frequency, leading to a good thermal stability for precise sensing applications, but cannot be fabricated into thin films. ZnO and AlN are the most popular materials for thin film devices nowadays. Among them AlN has the largest wave velocity and it is the only one whose deposition process has been industrialized. Moreover, it shows good mechanical property, good dielectric property and withstands high temperatures. Consequently, AlN enables the design of acoustic devices with higher operating frequencies and with improved sensitivity and better performance in harsh environments [19]. Figure 2 shows the crystal structure of AlN, the material under interest in this thesis.

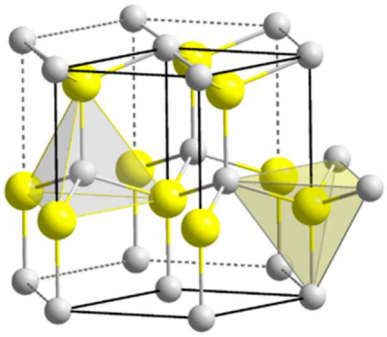

Figure 2: The crystal structure of AlN is the Wurtzite structure. The vertical axes(c-axes) is the one with the higher piezoelectric activity.

1.3 Bulk acoustic wave resonators and figures of merit

A BAW resonator consists of a piezoelectric material sandwiched between two metallic electrodes, as illustrated in figure 3.

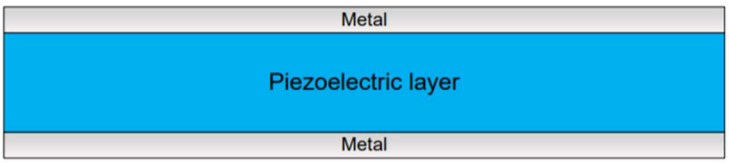

Figure 3: Structure of a BAW resonator.

From an electrical point of view, BAW resonators are capacitors with a dielectric material between their electrodes that has piezoelectric properties. The changes in the internal polarization of the material generate changes in its electrical impedance that can be measured with electronic instrumentation (as a network analyzer).

By applying an alternating voltage to the electrodes, acoustic waves are generated in the thickness of the piezoelectric material. These waves, that can have either longitudinal or shear nature, are reflected by both the upper and the lower electrode interfaces as depicted in figure 4. In this situation, the resonance condition is achieved when the excited and the reflected wave interfere constructively.

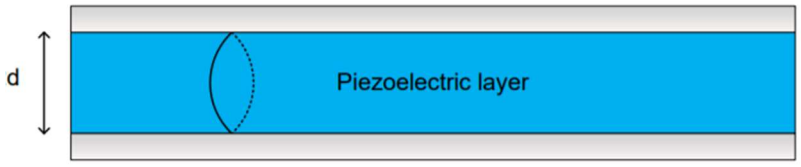

Figure 4: Standing wave formation in a BAW resonator.

The resonance frequency that carries out constructive interference is given by

$$f = \frac{v}{\lambda} = N\frac{v}{2d} \tag{7}$$

where v is the speed of the sound waves in the piezoelectric material, λ is the acoustic wavelength, d is the thickness of the piezoelectric plate and N is a natural number. With N equal to 1, the fundamental resonant frequency is obtained. As observed, the resonant frequency of the device is set

by the material proprieties and the geometry of the transducer. Changes in the surrounding medium can perturb the response of the resonator either by influencing the propagation of the waves in the material or by virtually varying the geometry. When a mass is attached to the surface of the resonator, its resonant frequency drops and can be monitored by the electrical output signal.

According to the equations proposed by Gunter Sauerbrey in 1959 [20], the resonant frequency shift Δf can be written as

$$\Delta f = S\Delta m \tag{8}$$

where Δm is the attached mass. The sensitivity S is defined as

$$S = -\frac{2 \cdot {f_r}^2}{A \cdot \rho \cdot v} \tag{9}$$

In this expression, f_r is the resonant frequency of the device, A is its area, ρ is the mass density of the piezoelectric material and v is the speed of sound wave in it. These expressions are only valid under simplified condition but explain well the basic operating principle of a BAW resonator.

The most typical example of a BAW resonator is a Quartz Crystal Resonator (QCR), illustrated in figure 5, in which the piezoelectric material is a single crystal of quartz.

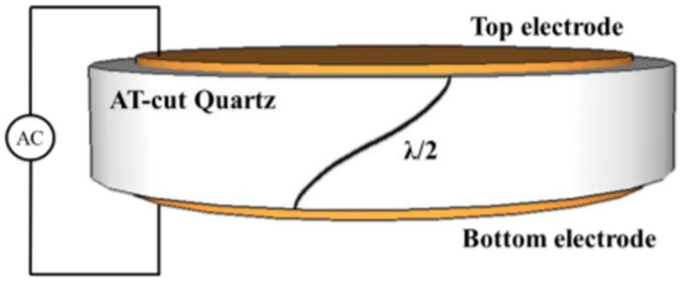

Figure 5: Structure of a QCR.

The resonance frequency of this kind of device is usually below 100 MHz, 200MHz in the best case, with a thickness of 8,3 µm [21]. This limitation comes from the fact that the physical thinning of the quartz crystal has reached its technological limit. As observed in equation (9) the sensitivity of a gravimetric sensor based on a BAW resonator increase with the resonance frequency of the device. This consideration drived the research towards the use of thin film of piezoelectric material for acoustic resonator, described in section 1.3.1.

A crucial parameter of a BAW resonator is the intrinsic electromechanical coupling coefficient k^2 of the piezoelectric material, described in the previous section. It describes the efficiency of the material in the conversion of the electrical energy in to mechanical energy. In addition to the electromechanical coupling coefficient k^2, the quality factor Q is frequently used to describe the performance of acoustic wave resonators, especially for the QCR and FBARs. The quality factor is usually defined as the ratio between the stored energy and the power dissipated per cycle and depends not only on materials properties but also on the device design. Indeed, the quality factor is influenced by dielectric losses of the piezoelectric materials, ohmic losses in contacts and electrodes,

acoustic leaks to the substrate, surface or interface roughness and surface finite lateral size of the resonator (which might generate undesired lateral modes).

These proprieties can be calculated from the electrical response of the resonator as a function of frequency. The impedance spectrum of a resonator, illustrated in figure 6, shows two narrow peaks, one at the resonant frequency f_r, where the modulus of the impedance has a minimum value, and another at the anti-resonant frequency f_a, where it assumes a maximum value. Moreover, at the resonant frequency, also known as series resonance, the phase of the impedance displays an abrupt shift from -90° to 90°, while at the anti-resonant frequency, or parallel resonance, it shifts from 90° to -90°.

The effective electromechanical coupling of the resonator can be easily calculated from the values of the resonant and anti-resonant frequencies. Among many different expressions to calculate its value, one of the more accurate is

$$k_{eff}^2 = \frac{\pi}{2} \cdot \frac{f_r}{f_a} \cdot \cot\left(\frac{\pi}{2} \cdot \frac{f_r}{f_a}\right) \tag{10}$$

often approximated with its second order Taylor series

$$k_{eff}^2 = \frac{\pi^2}{4} \cdot \frac{f_r}{f_a} \cdot \left(\frac{f_a - f_r}{f_a}\right) \tag{11}$$

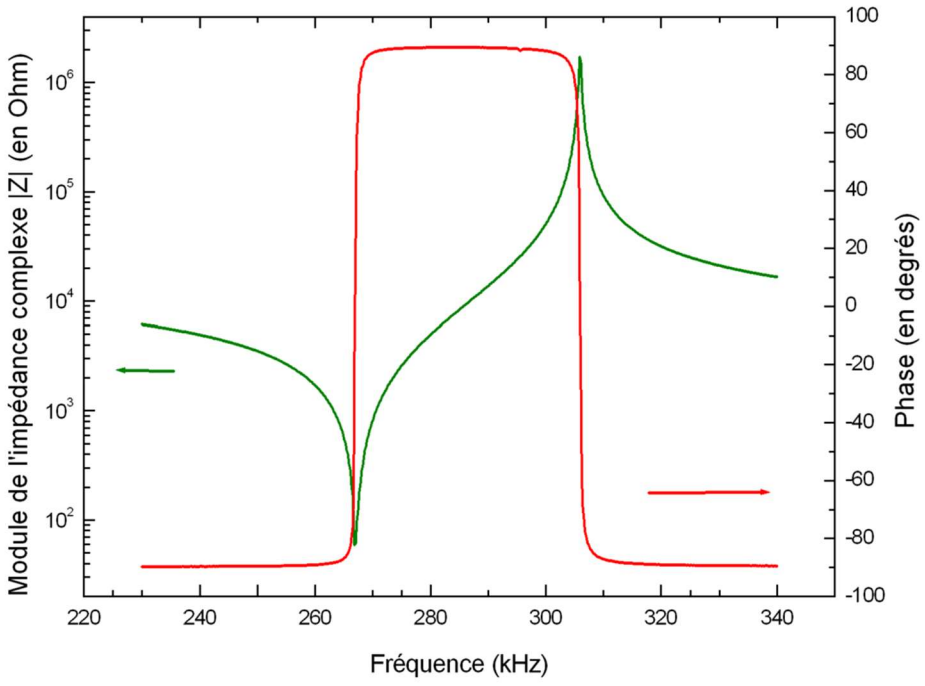

Figure 6: Typical Impedance spectrum of a BAW resonator.

It is important to understand that this effective electromechanical coupling differs from the intrinsic electromechanical coupling as it combines the influence of the material electromechanical property with other issues related to the device design. Although k^2 has a heavy influence on the value of k_{eff}^2, a resonator fabricated with a very high k^2 material can display a very low k_{eff}^2 if it is

not properly designed. Also the quality factor Q of the resonator can be easily calculated from its impedance spectrum as it is related to the abruptness of the resonance peaks. One of the easiest and more accurate expression to calculate is [22]

$$Q_{r,a} = \frac{f_{r,a}}{2} \cdot \left(\frac{d\angle Z}{df}\right)_{f_{r,a}} \tag{12}$$

To maximize the Q value is necessary to minimize all the energy loss in the resonator. There are many dissipation mechanisms in BAW resonators as heat dissipation by Joule effect in the resistive elements, as electrodes and contacts, or mechanical loses in the materials that surrounds the piezoelectric layer, but the main contribution to power dissipation is usually the acoustic energy loss due to leaking waves out of the piezoelectric layer. The term leaking waves refers to the acoustic energy loss due to its radiation towards the substrate (main mode) and the sides of the resonator (spurious lateral modes). In order to design a high Q resonator is therefore important to minimize the generation of spurious mode, e. g. designing properly the shape and dimension of the top electrode, and to acoustically isolate the resonator from the substrate, topic discussed in the following section.

1.3.1 Thin film Bulk Acoustic Wave devices.

The new standards imposed to EA devices regarding higher operating frequencies, monolithic integration and miniaturization cannot be fulfilled by using bulk single crystalline piezoelectric materials as in traditional QCM resonators. This limitation led to the birth of a new branch of BAW-based resonators, the thin film bulk acoustic wave resonators (FBARs), which can reach operating frequencies of several GHz. Depending on how the confinement of the acoustical energy in the resonant cavity of the device is achieved, FBARs are classified into two types: Free-Standing (or suspended) FBARs and Solidly Mounted Resonators (SMRs). In suspended FBARs, as in QCMs, the isolation is performed by the reflection at the electrode-air interfaces, while in SMRs the confinement is achieved by placing the resonator onto an acoustic reflector. The structures of these two kinds of resonator are illustrated in figure 7.

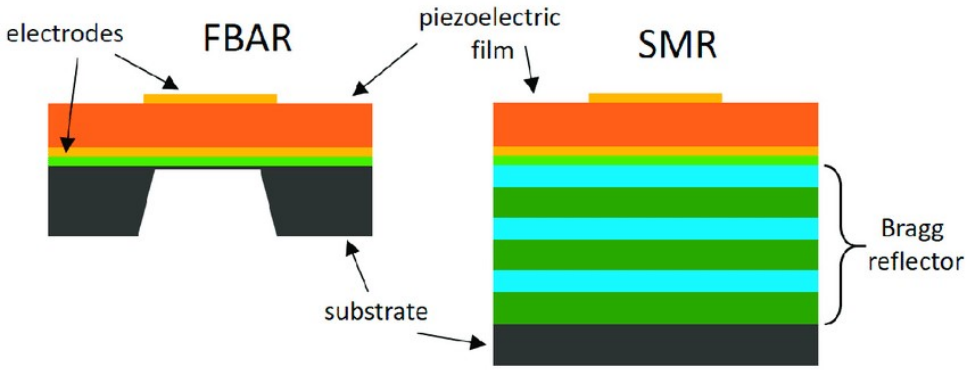

Figure 7: Free-standing FBARs and SMR structures. In the first case the isolation is performed by an air cavity, while in the second case the resonator is mounted on an acoustic reflector stack [23].

A crucial acoustical property of the materials involved in the fabrication of acoustic devices is the acoustic impedance. The acoustic impedance Z of a material is defined as the product of the sound velocity v in the material and its mass density ρ. It represents the opposition of the material to the sound propagation through it. When a travelling mechanical wave reaches an interface, the greater

the difference between the impedances of the two materials, the greater the amount of reflected energy, as described by the equation

$$r = \frac{Z_1 - Z_2}{Z_1 + Z_2} \tag{13}$$

where Z_1 and Z_2 are the acoustic impedances of the two materials and r is the acoustic reflection coefficient.

In Free-standing FBARs, the air cavity - that is obtained by micromachining techniques- has an acoustic impedance 30 times greater than that of the piezoelectric material, so almost all the acoustic energy is reflected at the interface, providing an effective acoustic isolation. On the other hand, the mechanical strength of the device is significatively compromised. In SMRs, the acoustic isolation is achieved by a reflector consisting on a stack of alternating high and low acoustical impedance materials with proper thickness, usually deposited by sputtering techniques. Currently, both structures are used to fabricate commercial devices with similar performances, but SMRs are more robust and they are less influenced by the environmental temperature (lower TCFs).

For the acoustic reflector, the most traditional setup is a stack of 5, 7, or 9 layers with quarter wavelength thickness, as in an optical Bragg mirror. This kind of structure can reflect up to 99.99% of the acoustic energy. A wide variety of materials is commonly used in the fabrication of the reflector stack for solidly mounted resonators. Table 1 lists the impedance of the main reflector materials. The most common combination are W/SiO_2 and Mo/SiO_2, but also fully metallic stack as Mo/Ti or fully dielectric stack as Ta_2O_5/SiO_2 have been investigated [21] [24] [25].

Table 1: Impedance of the main materials used for the fabrication of the acoustic reflector in SMRs [26] [27].

	Z [MRay]
Ir	120
W	101
Mo	63.1
Ta_2O_5	38.9
AlN	34
Ti	27.3
SiO_2	13.2

1.3.2 The shear mode

In FBARs, two types of acoustic thickness modes can be excited: longitudinal and shear mode. The longitudinal mode displays a mechanical deformation of the material in the same direction as the propagation of the wave, while in the shear waves the direction of deformation is perpendicular to the direction of propagation of the wave. Figure 8 illustrates the difference between these two types of vibrations. To excite the longitudinal mode, the AlN must be deposited in a highly oriented c-axis form, while for the excitation of the shear thickness mode, the AlN must be deposited with a tilted orientation.

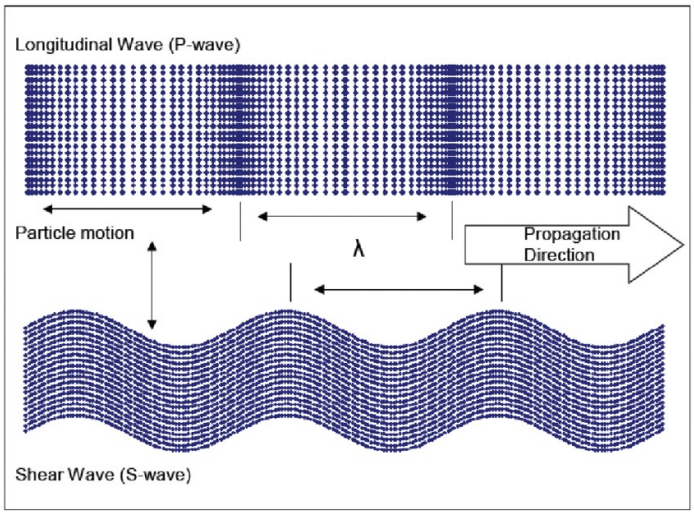

Figure 8: Schematic of the motion of the particles and the direction of propagation of waves in the longitudinal and in the shear modes.

Although devices can be designed by considering pure longitudinal and pure shear modes, this is only a close approximation. The generated modes in a material are actually quasi-longitudinal and quasi-shear [28]. That is, they have a small shear and longitudinal component, respectively, as illustrated in figure 9.

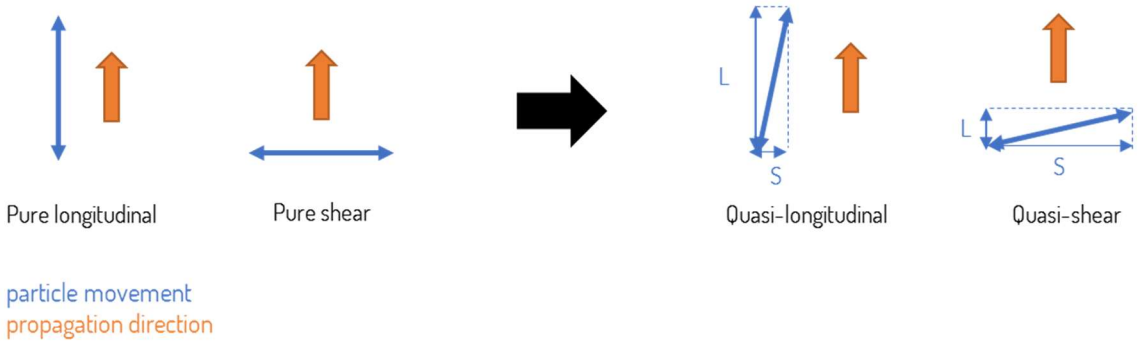

Figure 9: Representation of the direction of propagation and particle movement in quasi-longitudinal and quasi-shear modes excitations.

Traditionally, SMRs were developed as RF filters in the telecom industry operating in the longitudinal mode. However, for biological sensors they must work in the shear mode. Indeed, while in gaseous environment, traditional longitudinal mode SMR can be used, in-liquid sensing must be performed with shear mode resonators, as the shear waves do not couple with the liquid. This is not the case of the longitudinal mode, which couples to the surrounding liquid producing an acoustic leakeage that dramatically lowers the performance of the sensor (for example in terms of Q factor, as showed in figure 10).

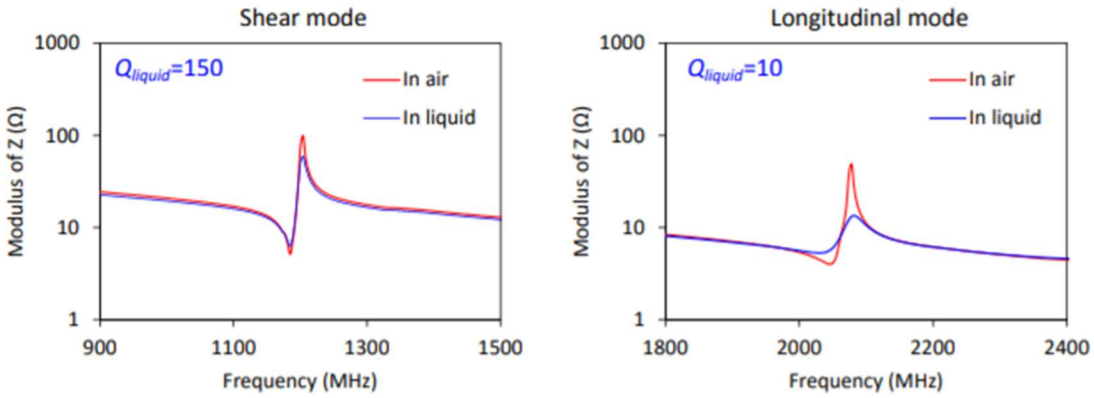

Figure 10: Quality factor in air and liquid of na SMR for the shear and the longitudinal mode [21].

1.4 Solidly Mounted Resonator as Biosensor

A biosensor is an electronic system able to generate an electric signal as response to a biochemical interaction that takes place on its surface, as illustrated in figure 11. The core of the biosensor is the transducer, which is responsible of the conversion of a physical variable into an electric signal. In order to be able to detect and quantify a particular molecule, the transducer must be functionalized by chemical recognition elements such as antibodies or enzymes. The principle of operation of a biosensor is quite simple. Thanks to the presence of the bio-receptors, some of the sensor properties will be altered by the presence of the target molecule. By tracking these properties, that can be either electrical, optical, or physical, the sensor is able to quantify the presence of the target species. Depending on the tracked property, biosensors are usually classified in electrochemical, optical, and gravimetric biosensors. In the electrochemical biosensors the transducer measures changes in voltage, current or resistance between two electrodes due to biochemical reactions that take place in the sensor in presence of the target specie. A typical example of an electrochemical biosensor is a pH sensor. On the other hand, optical sensors measure changes in the intensity or wavelength of the light emitted by the interaction of the sensor with the target. Gravimetric sensors, as BAW resonators, track the shift of the resonant frequency of a resonator due to the presence of a mass attached to its surface.

Beyond the property that they can track, biosensors have to fulfill strong requirements in terms of selectivity and sensitivity. They must be able to distinguish the target molecule from others present in the sample (selectivity) and must be able to produce a strong signal even in presence of really low concentration of the target molecule (sensitivity). Selectivity can be achieved by a proper functionalization, using antibodies, aptamers or any molecule that displays high affinity with the target specie. Sensitivity, on the other hand, depends mainly on transducer characteristics and the readout method used to collect the signal. In the case of EA resonator-based sensor, sensitivity is defined as the ratio between the frequency shift experienced by the resonator and the mass attached to its surface. Sometimes, this value is normalized to the resonant frequency when comparing different sensors in order to reduce the dependence of sensitivity on the operating frequency.

$$S = \frac{1}{f_0}\frac{\Delta f_r}{\Delta m} \tag{14}$$

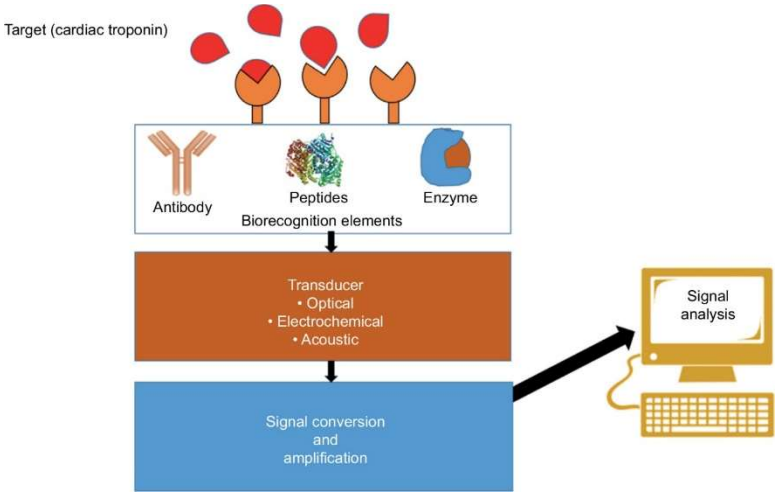

Figure 11: Schematic of the biosensor [39].

Other important characteristics of a biosensor are resolution, limit of detection (LOD), speed of response and stability. In the case of EA resonator-based biosensors, it is also important to consider some specific parameters of the resonator itself as the quality factor Q and the effective electromechanical coupling k^2_{eff}, presented in the previous chapter.

The process of functionalization was not included in this work. Nevertheless, it deserves a brief description. The term functionalization refers to the process used to deposit on the active area of a sensor chemical groups able to bind the target species. The reaction between the functionalized area and the target biomolecule should display high affinity to ensure a sufficient sensitivity and avoid false negatives, and high specificity, in order to avoid the detection of undesired molecules (false positives). Gravimetric sensors detect the target molecule by tracking the shift of the resonant frequency of the resonator due to the presence of a mass attached to its surface. For that reason, functionalization must provide bonds between receptors and target tight enough to ensure that the mass attached to the active area vibrate coherently with the resonator.

As reported before, an SMR-based biosensor must be designed to operate in liquid, as the biological particles to be detected can be found in biological fluids (as blood, for example). For that reason, the resonator must be optimized to operate in the shear mode. SMR have been widely studied as biological sensors and proved their potential in different works. However, the full optimization of their shear mode including device design, has never been performed. The most optimized mode so far has been the longitudinal mode as it is being used in RF filters for the telecom industry.

1.4.1 Fully dielectric acoustic reflector

To use an SMR as biosensor we need to place it in a fluidic setup leaving the electrical contacts dry outside while the active area of the device remains inside a sealing gasket through which we flow the biological liquids. The gasket is closed by an O-ring, as illustrated in figure 12.

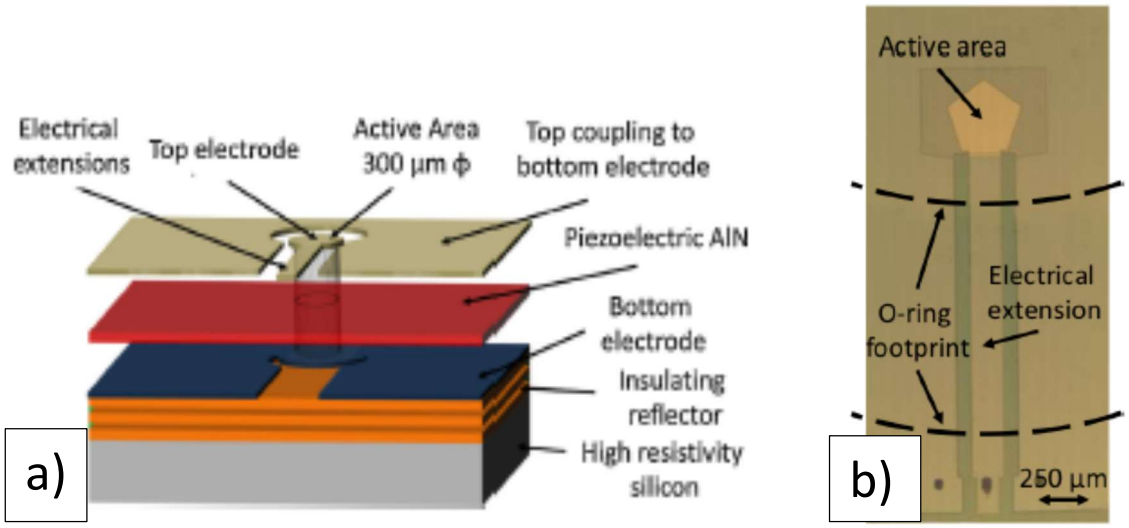

Figure 12: a) Schematic of the design of the resonator complete stack. The top and the bottom electrode are defined in such a way that no piezoelectric activity is generated out of the active area [29]. b) Illustration of the gasket closed by the O-ring that contains the active area [30].

Since we want only the active area to behave as a resonator, the device must be designed in such a way that the top electrode extension acts only as electrical paths. We need to define the bottom electrode only below the active area in order to confine the piezoelectric activity there, so we cannot have metallic layers in the acoustic reflector as they could act as bottom electrode of the extensions [29]. For that reason, a fully dielectric Bragg reflector must be designed.

The most traditional choice documented in the literature is a Ta_2O_5/SiO_2 stack. In this thesis, an AlN/SiO_2 was chosen as this combination of materials displays lower stress after the deposition of the stack.

1.4.2 Objective and optimization techniques

To use the SMR as a sensor, the resonant frequency is usually tracked by electronic means observing the maximum of the real part of the admittance or impedance. To perform an accurate measurement the resonant peak in the electrical response of the resonator must be as narrow as possible. In other terms, a resonator must display a high Q factor and the peak must be free of spurious modes, otherwise the result will be noisy and uncertain. Optimization is needed to achieve high performance SMR biosensor, and many techniques can be used, as was done in the past decades for the longitudinal SMRs used as filters.

These techniques have the main scope of improving the Q factor of the resonator by reducing the power loss in the device. As mentioned before, the main loss in the resonator is due to the acoustic energy leakage to the substrate, hence the optimization of the acoustic mirror is fundamental. The objective of this thesis is an optimization of the SMR technology for its use as biosensor, thus in a liquid environment. The main focus will be on the acoustic reflector optimization for the proper reflection of the quasi-shear mode, namely improving also the longitudinal component reflection present at the shear mode frequency. Two different approaches are proposed to improve the Q factors. These approaches are the Differential Grating Method and the Stop Band Theory [24], both

derived from optics. The resonator design and reflector performances will be simulated with a 1D Mason's model and with a 2D FEM analysis. The designed stacks will also be fabricated in order to verify the theoretical predictions.

2. Modelling techniques and theoretical methods

Modelling techniques are a fundamental tool when designing an electroacoustic resonator. On one hand, they allow designers to predict the response of a resonator. On the other hand, theoretical models are needed to properly fit experimental data to obtain the resonator parameters from its impedance measurements.

Two models are often used to design piezoelectric resonators: the Butterworth Van Dyke (BVD) model and Mason's model. The first one is a circuital model representing a resonator, but at microwave frequencies it only approximately describes the resonator [30]. For that reason, Mason's model is often chosen when modelling a thin film resonator. Mason model was used in this thesis to predict the response of the designed acoustic resonators.

Additionally, finite element modelling (FEM) was also used to refine the result, especially when considering the interaction of the resonator with the surrounding liquid medium.

2.1 Simulation with Mason's Model

Mason's model uses a transmission line concept in which the piezoelectric layer is a three-port network having two acoustic ports and one electric port, as illustrated in figure 13. The electrical impedance of the resonator at the electric port, as a function of frequency, can be calculated by applying the boundary condition at the acoustic ports [31]. In the case of an SMR resonator, the mechanical load on the left side represents the top electrode, while the right load represents the bottom electrode, the reflector stack, and the substrate. These elements are incorporated by using the network theory approach. Hence the boundary condition on the left side imposes that the stress is zero, while for the right side, z_r represents the effective mechanical impedance of the stack below the piezoelectric.

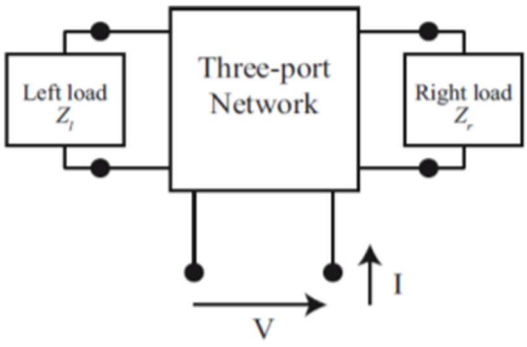

Figure 13: schematic of a one-dimensional three-port network Mason's Model for the piezoelectric layer.

Following the approach described by Lakin et al., the impedance at the electrical port can be given by [32] [33].

$$Z = \frac{1}{jwC_0}\left[1 - k^2 \frac{\tan\frac{kd}{2}}{\frac{kd}{2}} \cdot \frac{(z_t + z_b)cos^2\left(\frac{kd}{2}\right) + jsin(kd)}{(z_t + z_b)\cos(kd) + j(z_t z_b + 1)\sin(kd)}\right] \quad (15)$$

Where z_t and z_b represent the top and bottom acoustic impedance loads normalized by the piezoelectric acoustic impedance, d is the thickness of the piezoelectric plate, k^2 is the piezoelectric electromechanical coupling coefficient and C_0 is the physical capacitance described by εA/d with A being the active device area and ε the dielectric permittivity of the piezoelectric [34].

All structures attached to the piezoelectric plate, including the mechanical effect of the electrodes, must be described in terms of equivalent terminating acoustic impedance by the successive use of the transmission line equation:

$$Z_{in} = Z_0\left(\frac{Z_l + jZ_0\tan\theta}{Z_0 + jZ_l\tan\theta}\right) \quad (16)$$

The Mason's model together with the transmission line equation allows to calculate the transmission characteristics for longitudinal and shear waves, by just choosing the appropriate material parameters (acoustic impedance and wave velocity). On the other hand, it is not suitable to foresee spurious modes or other lateral acoustic effects and will also not predict the most accurate Q values.

For the reflector stack, the most convenient way to analyze it is by using the fundamental equation of the acoustic wave reflection and an interface:

$$r = \frac{Z_1 - Z_2}{Z_1 + Z_2} \quad (17)$$

being Z_1 and Z_2 the acoustic impedances of the materials at both sides of the interface. From that point of view, in an SMR structure, the reflection at the mirror interface with the resonator must be as high as possible (r ≈ 1), hence the total input impedance of the reflector stack must be either much smaller or much larger than that of the piezoelectric material. A more convenient way to characterize a reflector is by its logarithmic transmittance form:

$$T_{dB} = 10log_{10}(1 - |r|^2) \quad (18)$$

In this thesis a LabVIEW software implementing Mason's model was used. This model was previously implemented, and it allows an automatic calculation of the acoustic reflector thicknesses by providing it a desired resonant frequency and the values of densities and acoustic velocities for all layers. The software was designed to calculate an acoustic reflector centered for the longitudinal mode at a specific resonant frequency of around 1.9 GHz. The following equation is used to calculate the reflector thicknesses (t):

$$t = \frac{\lambda_{longitudinal}}{4} = \frac{v_{longitudinal}}{4f_r} \quad (19)$$

Since the longitudinal and shear velocities are related by a factor of around 1.6-1.7, the reflector will be centered for the shear mode at a frequency of approximately $f_{longitudinal}/1.6$.

For the resonant frequency to be tuned, after adjusting the acoustic reflector thicknesses, the software allows modifying the electrodes and piezoelectric material thicknesses. During this thesis the acoustic reflectors will be optimized by varying their standard thicknesses. Figure 14 shows a caption of the software where the densities, longitudinal velocities, and thicknesses of all layers of the SMR are observed. It also includes the logarithmic transmittance and reflectance of a resonator, as a function of frequency.

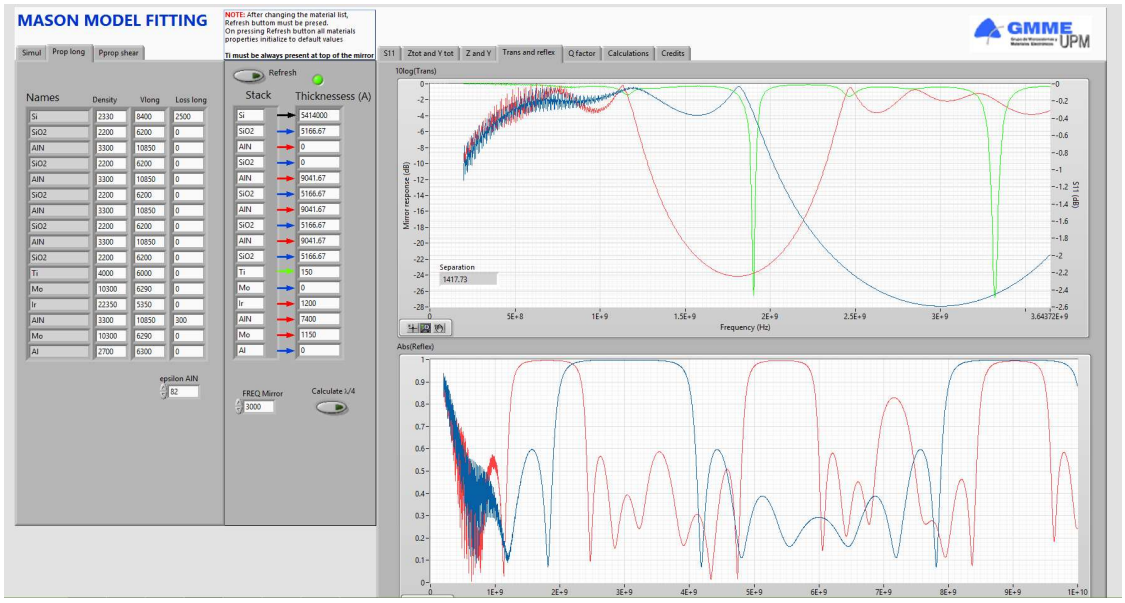

Figure 14: Caption of Mason's model software. On the right side the acoustic mirror response of an SMR. Red line is the transmittance of the shear waves, blue line is the transmittance of the longitudinal waves, green line marks the resonant frequencies of the resonator.

2.2. Finite element modelling

FEM is a numerical method to accurately solve any engineering or physical problem governed by differential equations. The great advantage is that it can couple many different physical phenomena that could be involved in a system by simultaneously considering their effects in the calculations. To solve a problem, the FEM subdivides a large system into smaller, simpler parts that are called finite elements. This discretization in the spatial dimensions is implemented by the construction of a mesh of the object. The mesh of the system is the numerical domain for the solution, which has a finite number of points.

For this thesis, a 2D FEM analysis was implemented. The advantage of this powerful tool is its ability to simulate the behavior of a resonator in a much more precise way and to calculate many more parameters of the resonator, as the displacement field within the resonator stack, showed in figure 15.

The model defines the AlN as a piezoelectric material with tilted grains, so the shear mode can be excited, and defines the electrodes and the layers from the acoustic reflector as elastic materials. It also includes a Si layer as substrate, which experimentally is a 4 inch Si wafer that has a thickness of 525 µm, however in the model only 10 µm are considered by placing a perfectly matched layer (PML) underneath, which completely absorbs the acoustic energy simulating the acoustic absorption that the thick Si wafer would produce.

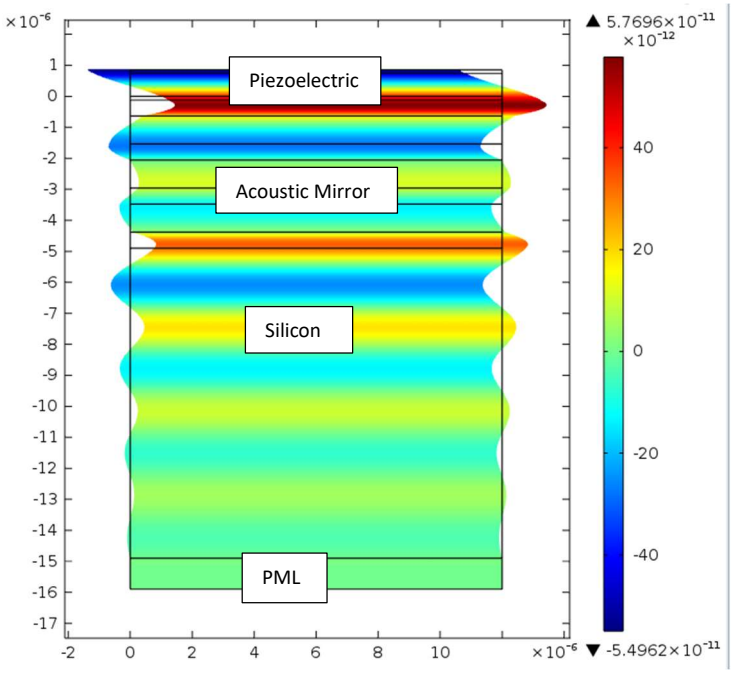

Figure 15: Shear component of the displacement in an SMR simulated with FEM analysis.

2.3 Acoustic mirror design

One of the main objectives of this thesis was to optimize the acoustic reflector of an SMR for its use as biosensor in a liquid medium. The materials chosen for the reflector stack where SiO_2 as low acoustic impedance material and AlN as high acoustic impedance material. The acoustic mirror used as a reference is a seven-layer, alternating low-high impedance, quarter-wavelength mirror, centered at a shear resonant frequency of approximately 1.8 - 1.9 GHz. The thicknesses of this reflector stack were easily calculated with the software as mentioned before. The shear acoustic velocity of the materials used (SiO_2 and AlN) and their thicknesses are listed in table 2.

Table 2: Shear velocity, shear wavelength at resonant frequency, and thicknesses of the layers of a 1.9GHz centered quarter-wavelength reflector stack, used as a reference.

Material	Shear velocity (m/s)	Thickness (µm)
SiO_2	3950	0.52
AlN	6170	0.91

This acoustic reflector provides optimal reflection of the shear waves (as seen in figure 14) since it fulfills

$$t = \frac{\lambda_{shear}}{4} = \frac{v_{shear}}{4f_r} \tag{20}$$

However, the optimal reflection of the longitudinal mode happens at a frequency 1.6 – 1.7 times higher. For that reason, such a centered acoustic stack provides almost total reflection for shear waves, but poor reflection of longitudinal waves, always presents in the main modes as they are quasi-shear, thus considerably lowering the Q value of the SMR.

For the optimized acoustic mirrors, two design approaches were investigated: the Diffraction Grating Method (DGM) and the Stop Band Theory approaches. Both methods are derived from optics and were previously proposed to optimize a longitudinal SMR for its use as filter [34].

Differential Grating Method approach

With the DGM we make use of higher order reflections: apart from the first order reflection at a quarter wavelength thickness ($t = \frac{\lambda_{shear}}{4}$), other higher-order reflections exist, corresponding to the layer thickness [24]:

$$t = \frac{\lambda_{shear}}{4} + m_1 \frac{\lambda_{shear}}{2} = (1+2m_1)\frac{v_{shear}}{4f_r} \quad (21)$$

Where m_1 is a non-negative integer and f_r is the resonant frequency of the resonator.

The same reflection condition exists for the longitudinal waves

$$t = \frac{\lambda_{long}}{4} + m_2 \frac{\lambda_{long}}{2} = (1+2m_2)\frac{v_{long}}{4f_r} \quad (22)$$

In these expressions λ_{shear} and λ_{long} are the wavelength of shear and longitudinal waves respectively, and v_{shear} and v_{long} are the corresponding velocities.

By making use of higher order reflections it is possible to find a thickness that matches the reflection conditions of both shear and longitudinal waves.

By combining equations (16) and (17) we find the expression

$$m_2 = \frac{m_1 - \frac{K-1}{2}}{K} \quad (23)$$

where

$$K = \frac{v_{shear}}{v_{long}} \quad (24)$$

These expressions are valid both in the low and in the high impedance layer.

By finding two integers that fulfill equation (18) and plugging them back to equation (16) the optimal thickness is calculated. Table 3 shows the calculated optimal thickness using this approach. Note that m_2 values are not exact integers, so that the reflection of longitudinal waves won't be properly centered at the considered frequency considered.

Table 3: Results of the DGM approach to design the optimized reflector.

	K	m_1	m_2	Thickness(μm)
SiO2	1.59	2	1.07	2.59
AlN	1.76	2	0.92	4.05

Stop Band Theory approach

To understand the Stop Band Theory approach it is required to start thinking at the problem in terms of phase drops along each layer. In a traditional quarter-wavelength stack (denoted LH, where

L stands for low and H for high impedance), the phase drops over both layers are π/2. It is possible to deviate from this equal phase drops and still obtain reflection bands. The Stop Band Theory says that a L(c·H)-stack (that is a stack where the ratio of phases drops over the low and high impedance equals an integer c) gives a maximum reflection for the frequencies at which the phase drop over the L-layer equals one of the so-called cardinal points φ_n:

$$\Phi_L = \varphi_n = \frac{n\pi}{1+c} \tag{25}$$

where n is an integer, n≤c and

$$c = \frac{\Phi_H}{\Phi_L} \tag{26}$$

where $\Phi_H \; and \; \Phi_L$ are the phase drops along the high and the low impedance layers.

Combining (20) and (21) we obtain that

$$\Phi_{TOT} = \Phi_H + \Phi_L = n\pi \tag{27}$$

To find the proper thicknesses that would reflect both shear and longitudinal waves, let's start defining c in terms of shear waves.

$$c = \frac{\Phi_{Hshear}}{\Phi_{Lshear}} \tag{28}$$

The phase drops of shear waves over the low and the high impedance layers can be written as

$$\Phi_{Lshear} = \varphi_n = \frac{n\pi}{1+c} \tag{29}$$

$$\Phi_{Hshear} = c\Phi_{Lshear} = \frac{cn\pi}{1+c} \tag{30}$$

The thicknesses of the low and high impedance layers relate to the shear wavelength by

$$t_L = \frac{\Phi_{Lshear}}{2\pi}\lambda_{Lshear} = \frac{n}{2(1+c)}\frac{v_{Lshear}}{f_r} \tag{31}$$

$$t_L = \frac{\Phi_{Hshear}}{2\pi}\lambda_{Hshear} = \frac{cn}{2(1+c)}\frac{v_{Hshear}}{f_r} \tag{32}$$

Where λ_{Lshea} and λ_{Lshea} are the wavelength of the shear waves in the low and high impedance layers respectively, and v_{Lshea} and v_{Hsh} the corresponding velocities.

The phase drops over these layers for longitudinal waves relate to their wavelength, or velocities, by

$$\Phi_{Llong} = 2\pi\left(\frac{t_L}{\lambda_{Llong}}\right) = 2\pi f_r\left(\frac{t_L}{v_{Llong}}\right) \tag{33}$$

$$\Phi_{Hlong} = 2\pi\left(\frac{t_L}{\lambda_{Hlong}}\right) = 2\pi f_r\left(\frac{t_H}{v_{Llong}}\right) \tag{34}$$

By combining (26) with (28) and (27) with (29), we can obtain

$$\Phi_{Llong} = \frac{n\pi}{1+c}\frac{1}{K_L} \quad (35)$$

$$\Phi_{Hlong} = \frac{cn\pi}{1+c}\frac{1}{K_H} \quad (36)$$

where K_L and K_H are the ratios between longitudinal and shear waves in the low and high impedance layer respectively.

To find the optimized thickness we must find an integer c, as low as possible in order to maintain a good fabrication simplicity, that will satisfy the condition (20), with n≤c. As the ratios K_L and K_H are not integers, it is actually impossible to find a low c that will fulfill exactly the condition of cardinal point. For that reason, we will try to fulfill the condition for shear waves, which are the primary waves modes in our resonator, knowing that the reflection condition for the longitudinal waves will be less perfect.

Table 4 shows the optimal thicknesses calculated using this approach by choosing a parameters c=2.

Table 4: Thicknesses and phase drops of the acoustic reflector optimized with the stop band theory approach.

	K	Thickness (µm)	$\boldsymbol{\Phi_{long}}$	$\boldsymbol{\Phi_{shear}}$
SiO_2	1,64	0,69	0,41π	2π/3
AlN	1,85	2,16	0,72π	4π/3
$\boldsymbol{\Phi_{TOT}}$			1,13π	2π

As mentioned before, since the total phase drop of longitudinal waves is not exactly a multiple of π, longitudinal waves reflection won't be maximum in this acoustic mirror. To further improve the performance of such an acoustic reflector, the phase error method can be used [34]. With this method, the thicknesses are optimized in such a way that the phase offset from the transmission minima (that is the cardinal point) for both longitudinal and shear waves are equal, hence the phase error is minimal in both cases [24].

A phase error Δϕ is introduced in equations (22), while keeping c and n values found before.

$$\Phi_{Lshear} + \Phi_{Hshear} = 2\pi - \Delta\phi \quad (37)$$

$$\Phi_{Llong} + \Phi_{Hlong} = \pi + \Delta\phi \quad (38)$$

Introducing K_L and K_H in (31) we obtain

$$K_L\Phi_{Llong} + K_H\Phi_{Hlong} = 2\pi - \Delta\phi \quad (39)$$

Summing (31) and (32) we find

$$(1+K_L)\Phi_{Llong} + (1+K_H)\Phi_{Hlong} = 3\pi \quad (40)$$

Finally, introducing the parameter c we obtain

$$(1+c+K_L+cK_H)\Phi_{Llong} = 3\pi \quad (41)$$

With this expression, we can now calculate the thickness of each layer that gives an equal phase error for both shear and longitudinal waves.

$$t_L = \frac{\Phi_{Llong}}{2\pi}\lambda_{Llong} = \frac{\frac{3}{2}}{1 + c + K_L + cK_H}\lambda_{Llong} \quad (42)$$

$$t_H = \frac{\Phi_{Hlong}}{2\pi}\lambda_{Hlong} = \frac{\frac{3}{2}c}{1 + c + K_L + cK_H}\lambda_{Hlong} \quad (43)$$

Table 5 shows the values of the thicknesses found with this method.

Table 5: Thickness values optimized with the phase error approach.

Material	Thickness (µm)
SiO_2	0,61
AlN	2,11

3. Experimental techniques

Although the full experimental part of the project had to be cancelled due to the pandemic situation, some devices could be fabricated. This chapter describes the fabrication techniques used and the electrical method to measure the devices. The fabrication of an SMR includes physical deposition methods to grow the thin films and photolithography to define the electrodes. Controlling the deposition parameters is crucial to obtain materials with the desired properties and to precisely control the thickness of the deposited layers.

3.1 High and ultra-high vacuum sputtering deposition

The sputtering deposition is a physical vapor deposition (PVD) technique based on the ejection of atoms from a target subjected to a highly energetic ions bombardment and their deposition on the substrate. The ions, typically extracted from a plasma, erodes the surface of the target by ejecting single atoms that subsequently condense onto the substrate surface creating a film. To deposit compounds, reactive sputtering can be performed. In this case, a reactive gas is added to the plasma atmosphere in the deposition chamber so that it reacts with the atoms ejected from the target before they condense onto the substrate.

Two reactive magnetron sputtering systems where used in this work: a high vacuum system for the deposition of the top electrode and the reflector layers, and a custom made ultra-high vacuum system specifically designed for the deposition of high quality piezoelectric AlN films. Both systems use pulsed DC plasmas.

The high vacuum system is mounted on a chamber pumped with a turbomolecular pump to the 10^{-6} – 10^{-7} Torr range. It uses 99.99% pure, 15 cm in diameter targets of Ti, Mo, Al, W, Ta and Si targets with a distance to substrate of 4.8 cm. It allows using different targets without breaking the vacuum, allowing multilayer deposition. The process parameters used during the deposition, listed in Table 6, were proven to be the ones that achieve a better adhesion between the different layers.

Table 6: Process parameters used during depositions.

Material	Oxygen	Nitrogen	Argon	Pressure (mTorr)	Power (W)
SiO2	25	-	4.2	1.6	1200
AlN	-	20.6	27.5	9	1200
Mo	-	-	18.1	2	400

The ultra-high vacuum system, presented in figure 16, is a dual chamber system. The first chamber, intended to load the sample, can be pumped in the 10^{-6}-10^{-7} Torr range in a short time, while the second chamber, the deposition one, is maintained under 10^{-8} Torr by a cryogenic pump. The AlN films are deposited here from a 15 cm target of 99.99% pure Al target in a reactive atmosphere of 60% of nitrogen in argon gas mixture. The target is located at 5.5 cm from the substrate, while the latter is placed on an insulated holder that allows biasing and heating.

The process to obtain tilted c-axis AlN films starts with the deposition of a 100 nm-thick seed layer of non-piezoelectric AlN grown at high pressure (5mTorr) and low power (600 W) to obtain mixed orientation. This is followed by an off-axis deposition at 1200 W and 1.6 mTorr with -65 V biased and 400°C heated substrate. The samples were held 5 cm far from the center of the substrate holder to obtain the desired grain tilt with respect to the surface. The combination of a non-ordered seed layer and the off-axis deposition has been proven to be the best way to obtain a good quality tilted c-axis AlN film [35]. Polishing the last layer of the reflector was founded to be crucial to obtain good quality piezoelectric films.

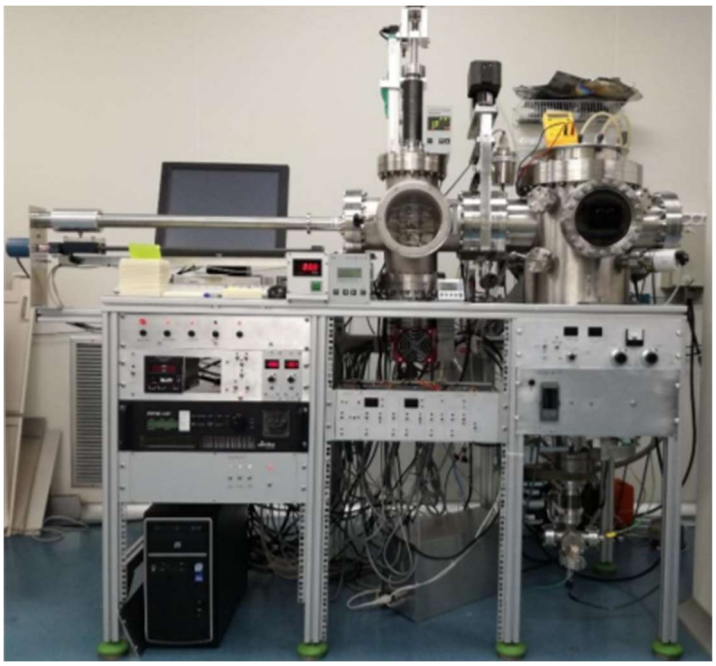

Figure 16: The ultra-high vacuum sputtering system used in this work.

3.2 Evaporation deposition

Evaporation is a PVD technique that doesn't involve the use of plasma. In this case the atoms are physically evaporated in vacuum by heating up the material under deposition. The vacuum allows the vapor particles to travel in the chamber freely and subsequently condense onto the surface of the substrate. The evaporation can be stimulated thermally by an electric filament (Joule effect) or by an electron-beam.

For the deposition of the 120 nm-thick iridium bottom electrodes, an electron-beam evaporation deposition was performed.

3.3 Photolitography

The patterning of the top electrode was achieved with a standard photolithographic process.

Photolitography is a microfabrication technique used to pattern a substrate that uses ultraviolet light to transfer the geometric pattern from a photomask to a chemical photoresist on the substrate surface. A series of chemical treatments then either etches the exposure pattern into the material or enables deposition of a new material in the desired pattern. This method enables the creation of extremely small features, down to tens of nanometers.

3.4 Fabrication route

The fabrication route chosen involves these main steps.

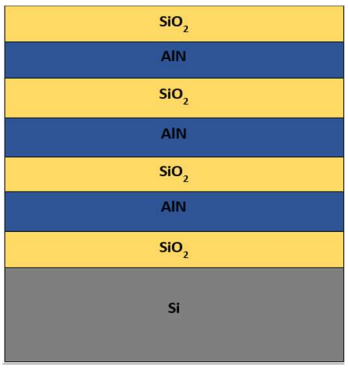

- **Sequential sputtering of alternating layers of AlN and SiO_2 over a thermally oxidized, high resistivity, (100) silicon wafer. The numbers and thickness of each layer depends on each acoustic reflector.**
- **Mechanical polishing of the last Sio_2 layer with 50 nm alumina powder and chemical cleaning of the surface.**

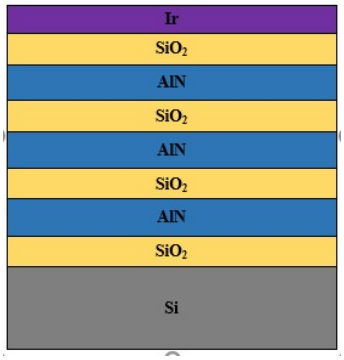

- **Sputtering of a thin 15 nm-thick Ti layer on the polished SiO_2 layer to improve the adhesion and e-beam evaporation of a 120 nm-thick Ir layer that will act as bottom electrode.**

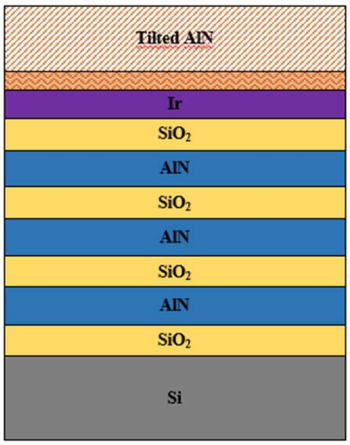

- **Sputtering of the seed layer and the 740 nm-thick tilted c-axis piezoelectric AlN.**

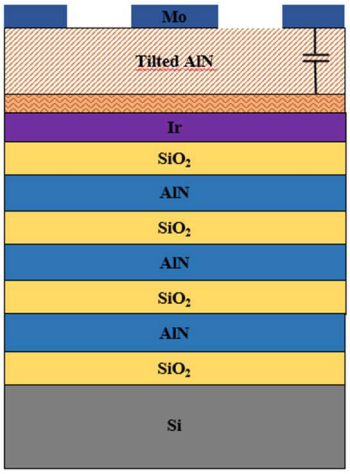

- **Sputtering of 115 nm-thick Mo film that will act as top electrode.**
- **Deposition of photoresist and standard photolithographic patterning. Wet Mo etching for top electrode definition. Photoresist removal.**

  The bottom electrode is accessed by a capacitive coupling.

3.5 Electrical characterization of the resonator

The electrical response of the devices has been tested by measuring scattering parameter S11 as a function of frequency. These measurements have been performed with calibrated GSG RF-probes for on-wafer contacting, using an Agilent N5230A network analyzer. The complex S11 parameter can be easily related to impedance values with the expression:

$$Z_{11} = \frac{1 + S_{11}}{1 - S_{11}} \tag{44}$$

where Z0 = 50 ohms corresponds to the system characteristic impedance.

4. Results and Discussion

4.1 Mason's Model 1D simulations

As already mentioned in the first chapter, the performance of a Solidly Mounted Resonator-based biosensor is determined by parameters as its sensitivity, selectivity, resolution, limit of detection and few more. While the selectivity arises from the accuracy of the functionalization process, the others arise mainly from the performance of the resonator itself. The two main parameters that describe the behavior of an SMR, and a piezoelectric EA device in general, are the quality factor Q and the effective electromechanical coupling coefficient k^2_{eff}. While the k^2_{eff} is particularly important for the use of an SMR as filter, Q is the main index of merit of an SMR used for sensing applications.

Our optimization process started, as mentioned, with the design of two acoustic reflectors. The thicknesses of the 7 layers of the stacks are summarized in table 7. It is worth remembering that each stack has 4 SiO_2 layers and 3 AlN layers. From this point of the text, we will refer to the mirrors as reference (REF), differential grating method (DGM), and phase error (PH), based on the structures described in section 2.1.3.

Table 7: Summary of the thicknesses of the 3 simulated acoustic mirrors.

	SiO_2 thickness (µm)	**AlN thickness (µm)**
REF	0,52	0,90
DGM	2,59	4,05
PH	0,61	2,11

These new, optimized stacks, are meant to reflect both shear and longitudinal waves in order to improve the performance of the resonator by lowering the acoustical loss towards the substrate, thus increasing the quality factor Q. By simulating the optimized stacks with Mason's model, the mirror response was calculated.

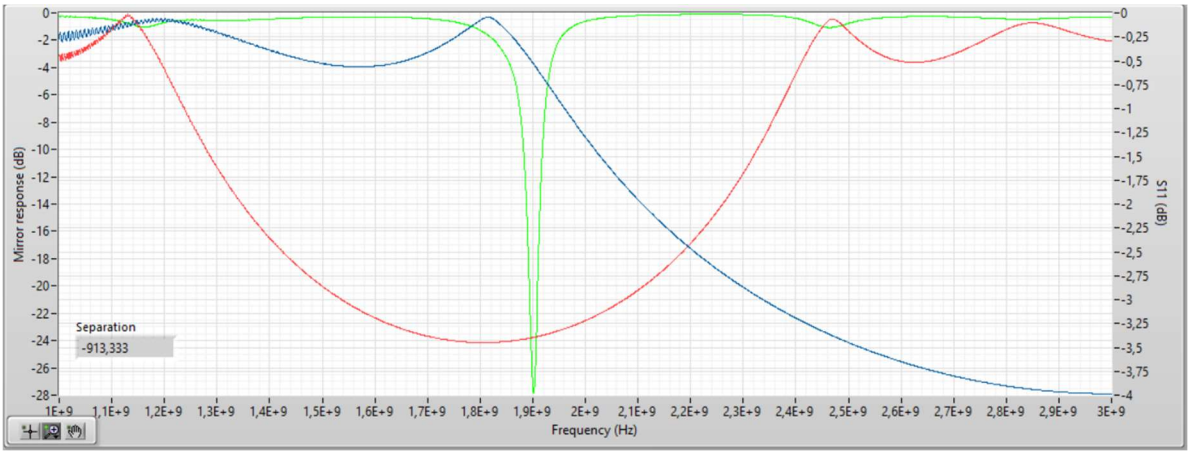

Figure 17: Reference mirror transmittance in dB: the blue line is the transmittance of the longitudinal waves while the red line is the transmittance of the shear waves. The green line represents the resonance peak of the shear mode.

In figure 17, the response of the reference mirror is presented. It is quite clear that the REF mirror was a good reflector for the shear waves, the principal mode in the resonator, but was a terrible reflector of longitudinal waves, always present to some extent in a quasi-shear mode of vibration. This can be noticed since the transmittance of the shear wave at the resonance frequency is minimum, hence the energy is properly reflected back, but for the longitudinal is much higher. The reason for the low reflection of the longitudinal mode comes from the quarter-wavelength design centered for the shear waves.

The optimized acoustic mirrors, on the other hand, show a clearly better response as they maintain an optimal reflection of the shear waves while significantly improving the reflection of the longitudinal waves, as presented in figure 18 and figure 19. In particular, the DGM approach turns out to be the best one in terms of reflection of both shear and longitudinal waves as it has the minimum transmittance at the resonance frequency.

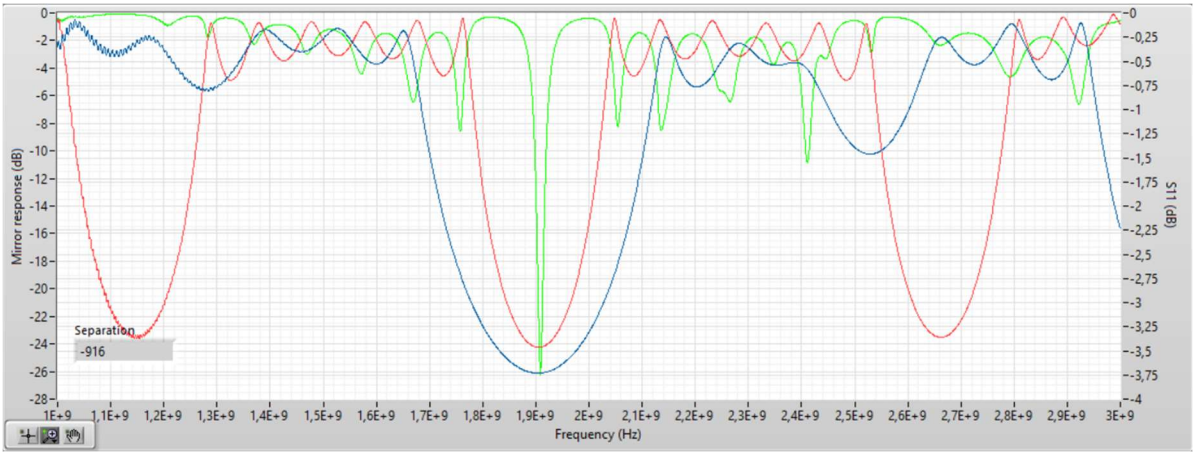

Figure 18: DGM mirror transmittance in dB: the blue line is the reflectance of the longitudinal waves while the red line is the reflectance of the shear waves.

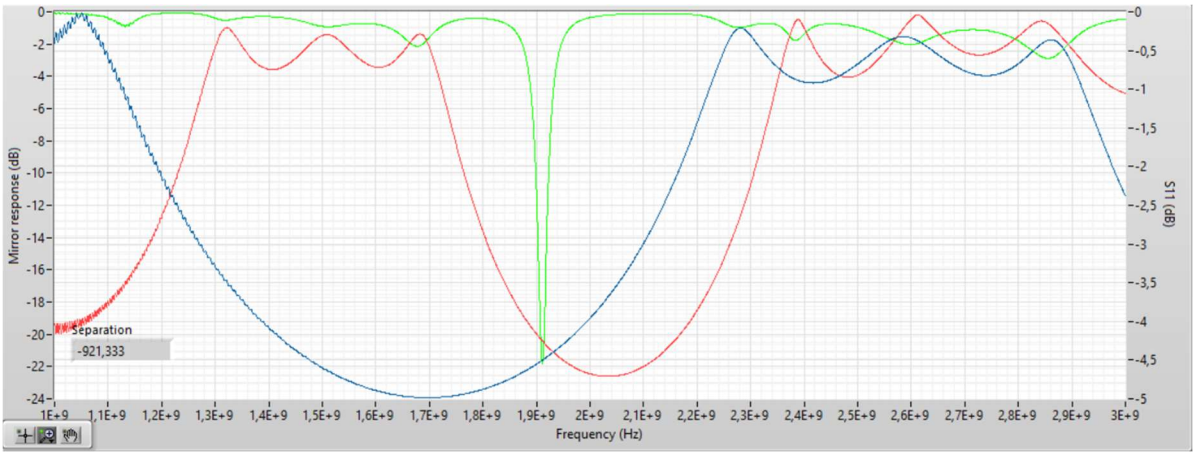

Figure 19: PH mirror transmittance in dB: the blue line is the reflectance of the longitudinal waves while the red line is the reflectance of the shear waves.

In table 8 the values of transmittance of the three simulated acoustic mirrors together with the device performance (Q and k^2_{eff}) are listed.

Table 8: Reflectance of the reference and optimized mirrors. Quality factors and effective electromechanical coupling coefficient of the resonators calculated with Mason's model.

	Shear waves transmittance (dB)	Longitudinal waves transmittance (dB)	Q factor at resonance	k^2_{eff}
Reference	-23,8	-4	286	3,22
DGM	-24	-26	489	2,21
Phase Error	-20,5	-22	306	2,96

Besides the transmittance of the acoustic reflectors, with Mason's model we can also extract the electrical impedance of the resonator, or its inverse- the admittance- as a function of frequency. It is then possible to observe the sharpness of the resonant peak and to quantify the performance of the resonator by calculating its Q factor. It is worth mentioning that the sharpness of the resonant peak is fundamental for its tracking during a sensing process. To extract the Q values with this model we first set, in the REF mirror, a loss factor in the active AlN layer that produces a Q factor of around 300, according to precedent experimental results of our laboratory [10]. Mason's model is a 1D Model that doesn't take into account all types of loss sources, e.g. spurious modes in the lateral-2D dimension, hence we had to assume that all the power dissipated by the device was loss through acoustic leakage towards the substrate or the damping loss in the piezoelectric layer. Then we maintained this loss value for the two optimized devices to obtain a reliable comparison.

The values obtained are listed in table 8, where we see that the better response of the designed mirrors raises the Q values of the optimized stack. On the other hand, the effective electromechanical coupling coefficient is lowered as an effect of the bigger thickness involved in the acoustic mirrors of the optimized ones. Since as the Q factor raises the k^2_{eff} tend to reduce, a common way to compare the performance of different SMRs is to observe the value of the product of these two parameters. In this case, the index of merit $Q\cdot k^2_{eff}$ of the reference, calculated with Mason's model, turns out to be higher than that of the Phase Error optimization, but lower than that of the DGM optimization. Anyway, this is not so relevant as for sensor applications the quality factor is the best parameter to evaluate the performance of the device.

Although the result show that he device of the performance can be optimized through a proper design of the acoustic reflectors, it is worth mentioning that these stacks contain thicker layers, which can be a disadvantage from a fabrication point of view. The fabrication of such thicker layers is more complicated, requires more time, and could lead to thermal stresses and adhesion problems. However, the fabrication of the optimized acoustic reflector in the lab proved by depositing the material with proper conditions the adhesion and thermal stress issues can be solved. Additionally, the presence of these thicker layers in the acoustic mirrors can produce undesired resonances around

the main resonant peak. This issue is particularly evident for the DGM optimized reflector and can be observed in the impedance spectra of the devices, showed in figure 20.

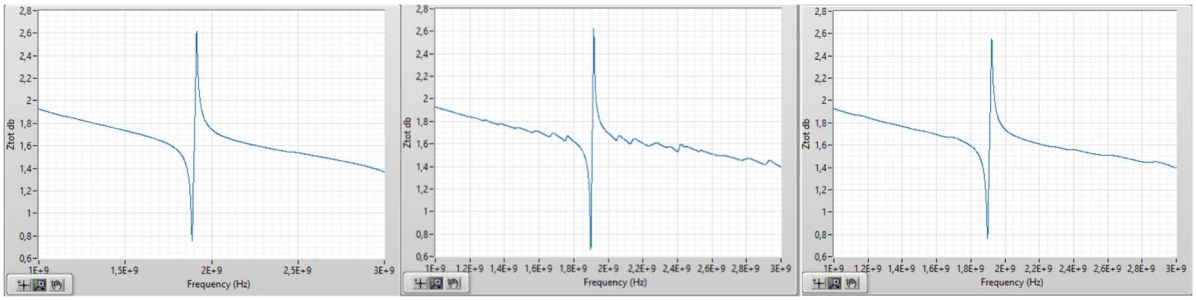

Figure 20: Impedance spectra of the Reference (left), DGM (center) and Phase Error (right) mirrors.

As seen, Mason's Model is a powerful tool to calculate the response of a resonator in terms of reflectance of the mirror, impedance spectrum and figures of merit as Q factor and k^2_{eff} . However, its 1D nature does not allow the prediction of any lateral phenomena, nor the response of the resonator in a liquid medium. The behavior of these devices when interacting with a liquid medium is crucial for their application as biosensors. For that reason, a further analysis of the optimized stacks was performed with FEM analysis.

4.2 Finite Element 2D simulations

These simulations were performed in order to complete and have a better insight of the preliminary results obtained by Mason's model. By using FEM analysis, it was possible to calculate their behavior in terms of electrical response, mechanical-acoustical energy confinement in each part of the stack and interaction with liquid.

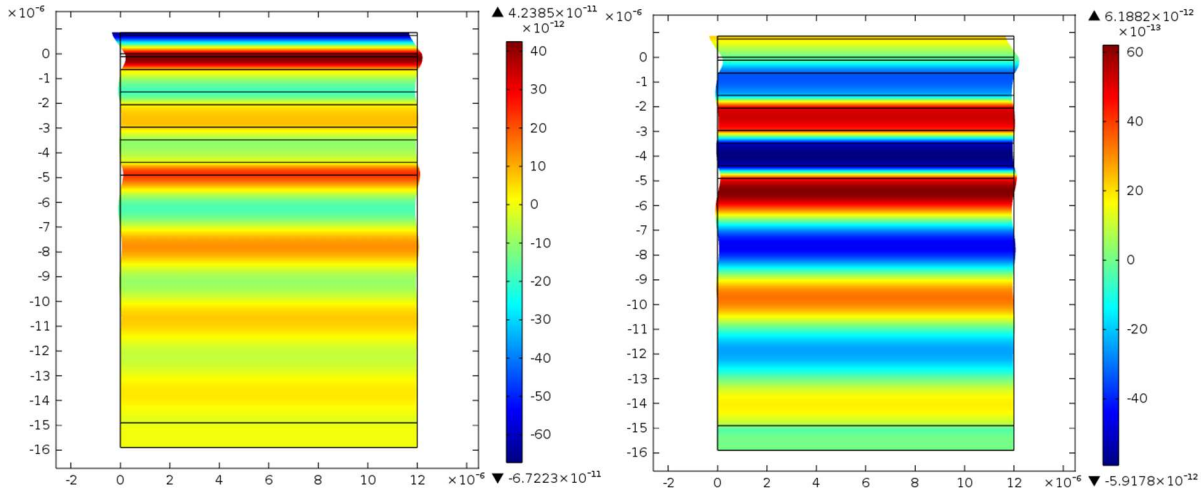

Figure 21: Displacement fields in the REF resonator. On the left the shear displacement, on the right the longitudinal displacement.

The confinement capabilities of the acoustic mirrors were analyzed by simulating the displacement of the particles in the resonator during its vibration at resonance. By observing the magnitude of the displacement in each layer of the stack it is possible to deduce how much of the acoustic energy is

confined in the piezoelectric layer and how much is lost towards the substrate. In figure 21, both the shear and the longitudinal displacements of the reference resonator are shown.

As observed in figure 21, the REF acoustic stack confines in the piezoelectric layer a big proportion of the shear component, while the longitudinal component is mainly lost towards the substrate. This arises directly from the low reflectance of the longitudinal waves of the stack.

In figure 22 and 23, the displacement field of both shear and longitudinal waves of the optimized stacks are presented.

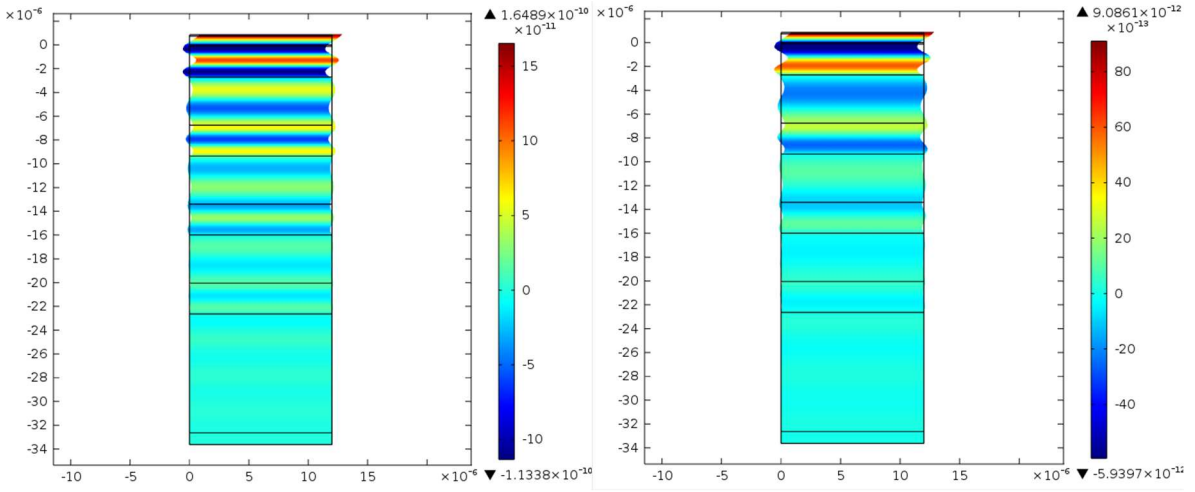

Figure 22: Displacement fields in the DGM resonator. On the left the shear displacement, on the right the longitudinal displacement.

From the displacement fields of the DGM resonator we extract that the improvement of the Q factor arises from the dramatically improved energy confinement of the longitudinal component. This agrees well with the transmittance of the DGM reflector from figure 18.

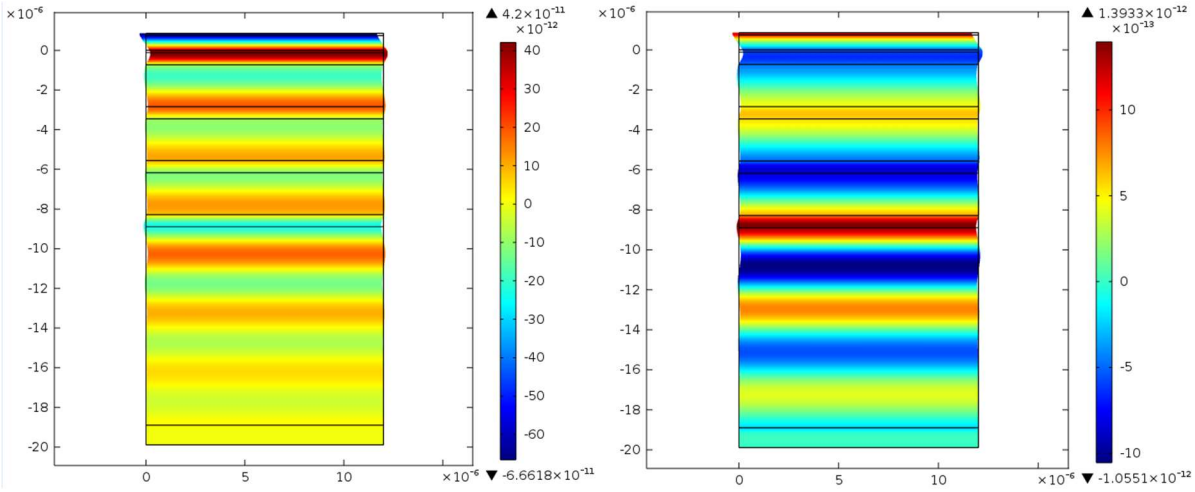

Figure 23: Displacement fields in the PH resonator. On the left is represented the shear displacement, on the right the longitudinal displacement.

Regarding the PH optimized stack, things appear to be less exciting. The confinement of the longitudinal waves turns out to be just slightly improved, compared to the REF one.

A more precise and quantitative way to approach the problem is to calculate the Q factors of the devices from their simulated electrical responses. Figure 24 displays the admittance response and the current flow as a function of frequency of the three resonator. The inward current density represents here the real part of the electrical admittance.

As can be qualitatively observed in figure 24, the optimized resonators display a sharper resonance, sign of a better performance. Quantitatively, we chose to calculate the Q factor from the sharpness of the resonant peak in the current density spectrum with [36]:

$$Q = \frac{f_r}{f_{+3dB} - f_{-3dB}} \tag{45}$$

Where f_{+3dB} and f_{-3dB} are the frequencies at witch the current density is 3 dB lower than the maximum value, and f_r is the resonance frequency. Table 9 shows the Q values obtained with this method.

Table 9: Quality factor predicted with the FEM simulation of the three resonators.

Resonator	Quality factor
REF	294
DGM	455
PH	351

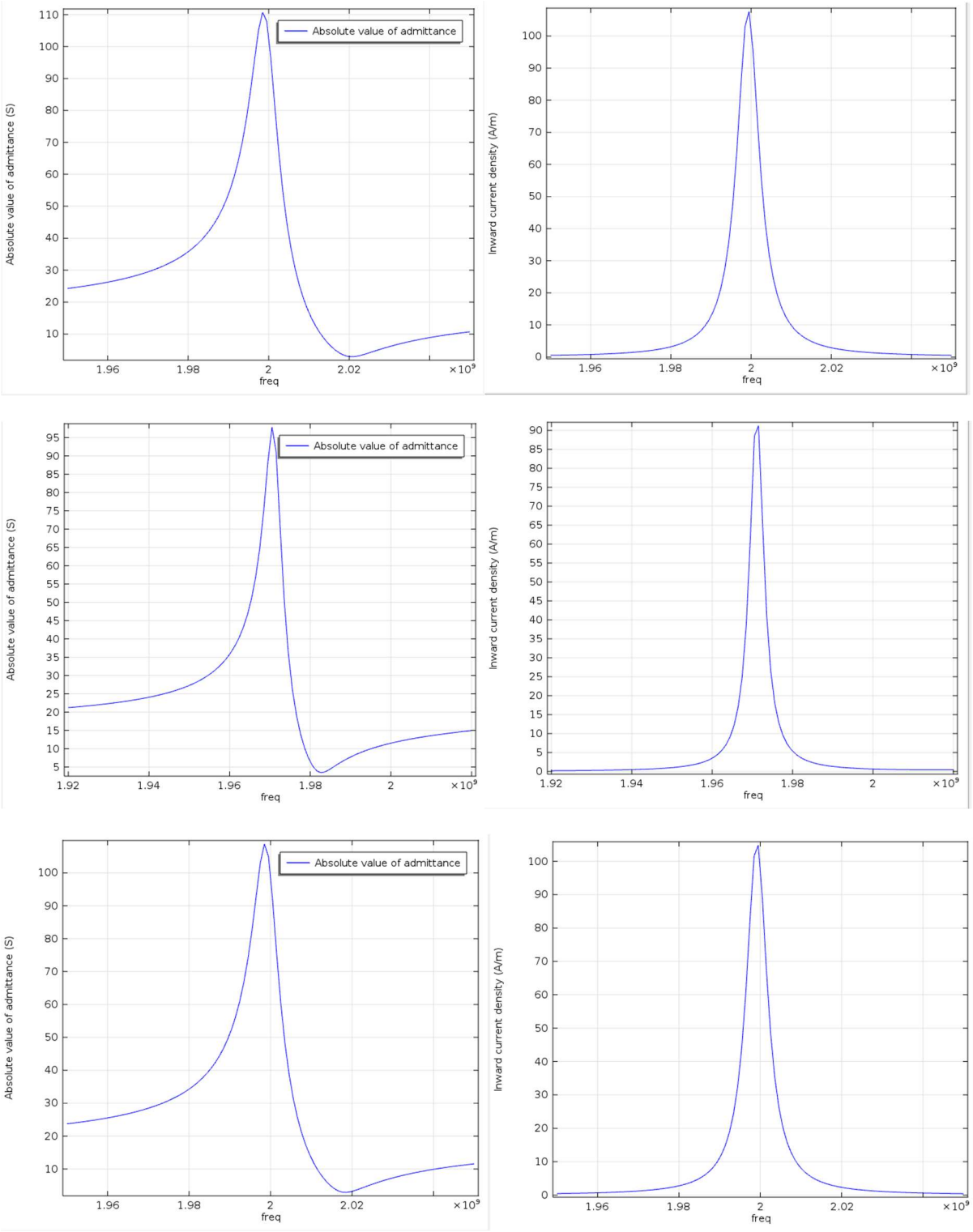

Figure 24: Electrical resonse of the three resonators (from the top: Reference, DGM and PH). On the left, impedance spectrum is represented. On the right, the real part of the current density flowing throug the resonator is shown.

As predicted also with Mason's model, the Differential Gratings Method appears to be the best approach to optimize the reflector stack by preventing the acoustic loss of the longitudinal component

and consequently improve the performance of the resonator in terms of Q factor. The Q factor of DGM appears to be roughly 50% higher compared to the reference one, which means a remarkable improvement. The phase error optimized stack displays a lower quality factor, but always higher than that of the reference. On the other hand, as already outlined, the presence of thicker layers in the DGM stack introduces additional resonances, which we also observe with this model. Figure 25 shows the impedance spectra of the two optimized resonators on a wider range. The DGM approach produces a sharper peak, but more undesired resonances.

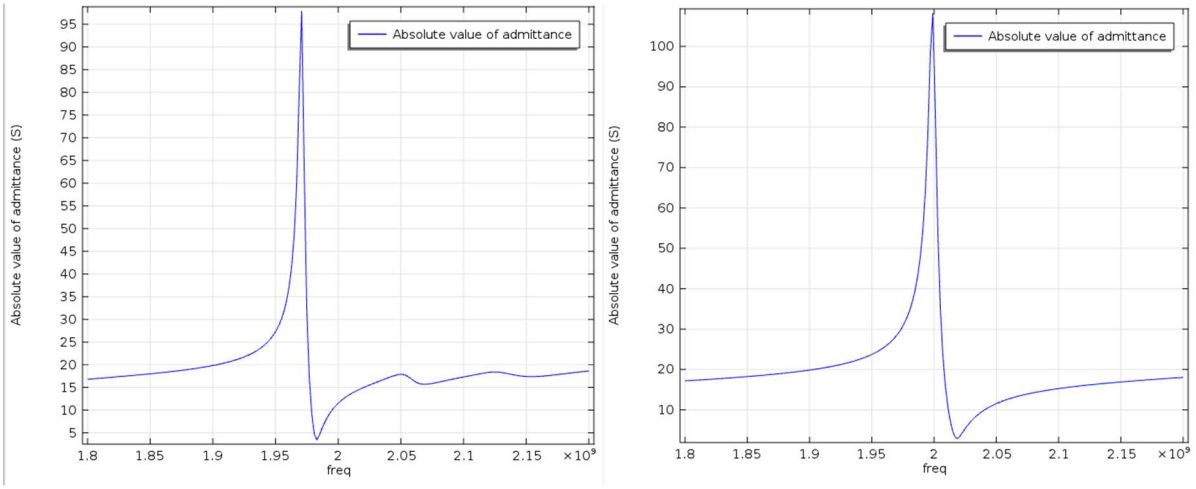

Figure 25: Admittance spectra of the DGM (left) and the PH (right) resonator.

4.3 In liquid Finite Element 2D simulations

The last step related to smulations was to predict with FEM analysis their behavior in a liquid medium. In this case, a previousy designed model for the liquid layer was employed [37]. A 10 µm-thick layer of liquid was defined over the surface of the resonator, with a perfectly matched layer on top that absorbs all the acoustic energy to simulate the actual larger extension of the liquid.

By calculating the quality factor Q in the same way as in the previous section, we can quantify the performance of the three resonatosr in a liquid enviroment. Table 10 shows the quality factor calculated from the sharpness of the resonant peaks with FEM with and without the liquid.

Table 10: Quality factor comparison with and without the liquid.

Resonator	Q factor in air	Q factor in liquid
Reference	294	193
DGM	455	299
Phase Error	351	218

The presence of the liquid lowers the performance of the resonators as a higher fraction of the energy contained in the device is lost towards the liquid, as observed in figure 26 for the DGM resonator. The shear component of the waves doesn't couple to the liquid. Conversely, the longitudinal component propagates through the liquid, lowering the performance of the resonator.

Despite the expeted coupling of the longitudinal component to the liquid in all cases, the optimized stacks maintain their higher performance as compared to the REF on. The DGM approach turns out

again to be the best method. Its performance in liquid is even slightly better than the performance of the REF resonator in air.

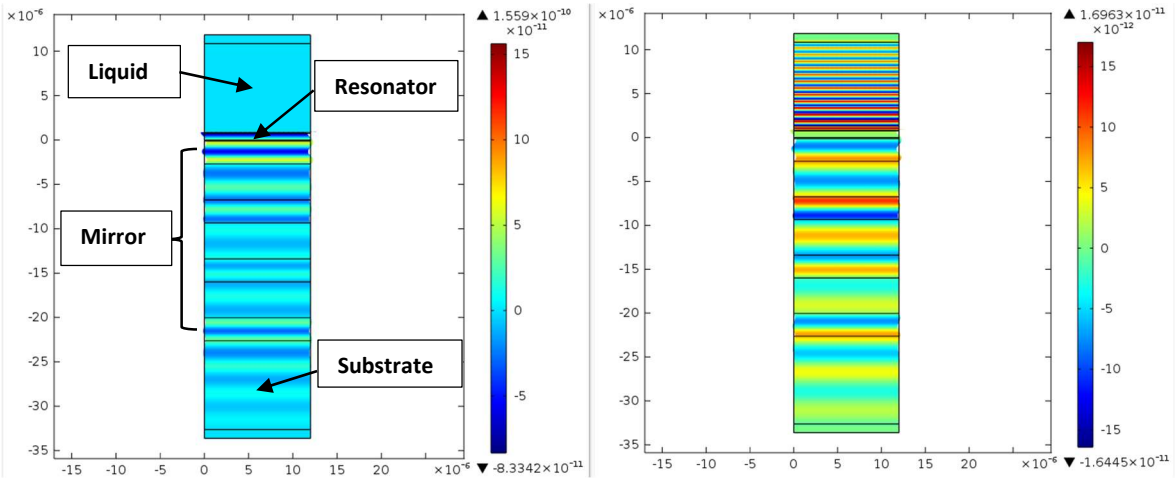

Figure 26: Displacement field in the DGM optimized resonator. Shear displacement on the left, longitudinal displacement on the right.

Figure 27 shows a comparison between the current density response (real part of admittance) with and without the liquid for all resonators. The presence of the liquid medium degrades the peaks by widening them, which results in lower Q values.

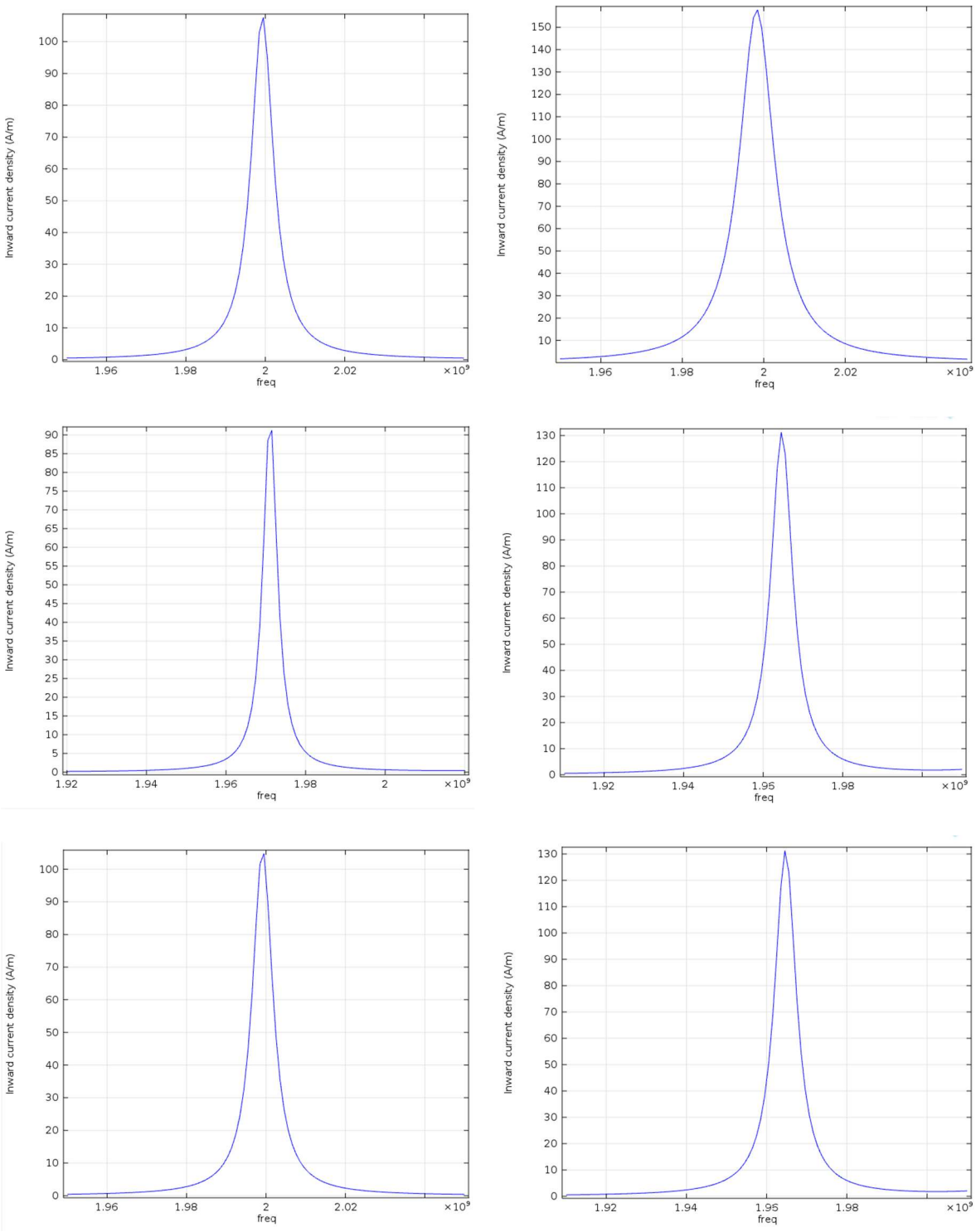

Figure 27: Current density spectra for the three resonator without (left) and with the liquid (right). From the top: Reference, DGM and Phase error.

4.5 Fabricated devices

The initial idea of this thesis was to fabricate the proposed devices, optimize them with different tecniques and finally measure them in a liquid medium. However, only few devices could be fabricated with no time for propoer optimization. Nonetheless, it is worth showing the preliminary results from the initial attempt to fabricate all three SMRs.

Figure 28 shows the electrical impedance of the REF, the DGM and the PH resonators. Firstly, we observe that the resonant frequencies are shifted from the designed ones. Many factors can affect the value of the resonant frequencies, including thicknesses of all the deposited layers or their acoustical properties (density and acoustic velocity). To perfectly adjust the resonant frequencies, several calibrations of the machines and materials should be performed. Even if the materials were not perfectly calibrated at these initial measurements, the Q factor could be extracted. Their values are shown in table 11.

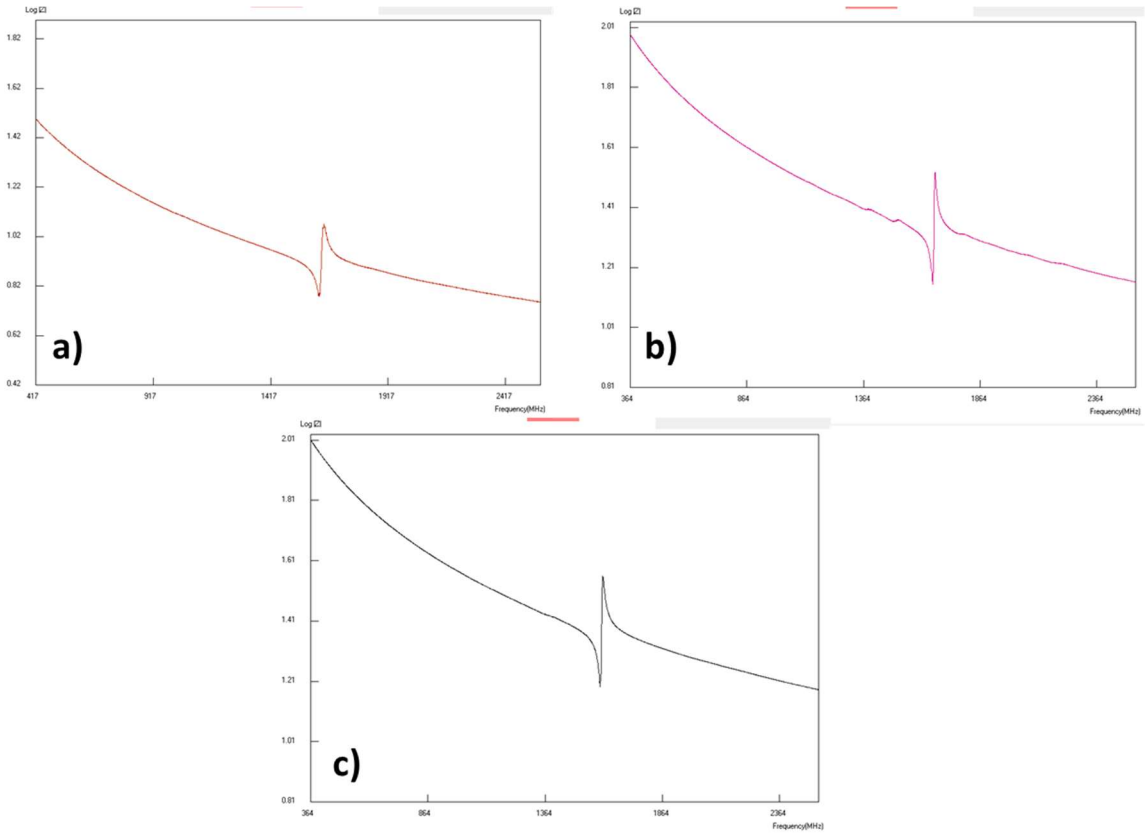

Figure 28: Electrical impedance of the fabricated devices. a) REF design, b) DGM design and c)PH design .

The measured Q values are much lower than the simulated ones and the explanation is the fact that the thicknesses of the deposited layers are deviated from the desired ones, hence the transmittance of the reflectors is different from the predicted one. This eventually implies that the resonant peak is not perfectly centered at the optimum frequency value as expected in figures 17, 18 and 19. To perfectly adjust the resonant frequency and center them, more experiments are needed.

Table 11: Experiemntal quality factors for the three resonators.

Resonator	Quality factor
REF	61
DGM	102
PH	99

Nevertheless, even the Q values are lower than expected, we can still see the improvement in the DGM design compared to the REF one.

5. Conclusions and Future work

5.1 Conclusions

After evaluating the results obtained during the development of this project, the conclusions and possible lines of future research are stated.

- Two techniques were employed to optimize the acoustic reflectors of shear mode solidly mounted resonators for their use in liquid as biosensors. The aim was to improve the reflection of the longitudinal component in the acoustic reflector. This component is always present in quasi-shear modes and its radiation towards the reflector produces acoustical losses.
- The optimization of the acoustical mirror was performed with two different approaches, both derived from optics: the Differential Gratings Method and the Phase Error Approach. Both methods were tested through simulations using the one-dimensional Mason's model and two-dimensional Finite Element Method analysis.
- Both DGM and PH methods appeared to considerably improve the performance of the SMR by increasing the reflectance of the longitudinal component in the acoustic mirror, while keeping optimal reflection of the shear component. The enhanced performances of the optimized acoustic reflectors remarkably reduce the acoustical energy loss towards the substrate. This translates to higher Q factors compared to a standard design.
- The best optimization approach turns out to be the DGM, improving the Q factor of about 50%.
- The superior performance of the DGM devices was also demonstrated with FEM analysis in a liquid medium.
- Although the performance of the device was improved, with these two methods thicker layers for the acoustic reflector are needed. This can promote lower adhesion and thermal stresses in the stack. However, an initial fabrication of these devices proved that by properly depositing the materials this issue can be controlled.
- The experimental measurements of the devices that could be fabricated verified the simulated results by showing again that the DGM method improves the Q factor of the SMRs. Although the Q values were lower than predicted, this can be solved by adjusting the thicknesses, calibrating the material deposition processes, and performing several depositions.
- These theoretical and experimental results are useful for the design and fabrication of shear mode SMRs for their use as biosensors in liquid media.

5.2 Future work

Since the pandemic situation prevented the optimal fabrication of the designed devices, more experimental tests need to be performed. The results obtained in this work open the way for further futures studies to finally boost the SMR-based biosensor technology. The suggested future research lines are listed below.

- Test the DGM and PH optimized devices in a real liquid media.
- Perform real biosensing experiments.
- Reduce the presence of spurious modes, especially in the DGM design, by employing techniques like the deposition of an edge ring on the top electrode or the apodization.

Bibliography

[1] R. Aigner, "SAW and BAW technologies for RF filter applications: A review of the relative strengths and weaknesses," Beijing, 2008.

[2] R. Aigner, "Actuators and Microsystems, 2005" in *The 13th International Conference on Solid-State ,* North Corea, 2005.

[3] K. M. Lakin, "Thin film resonators and filter" in *1999 IEEE Ultrasonics Symposium. Proceedings. International Symposium*, 1999.

[4] M.Schmid et al., "Sensors based on piezoelectric resonators", *Sensor and Actuators a: Physycs,* vol. 41, pp. 1-21, 1995.

[5] G. Wingqvist et al., "Shear mode AlN thin film electroacoustic resonator for biosensor applications" in *SENSORS, 2005 IEEE*, Irvine, 2005.

[6] M. Benetti et al., "Microbalance chemical sensor based on thin-film bulk acoustic wave resonators" *Applied Physics Letters,* vol. 87, 2005.

[7] A. Arnau, Piezoelectric Transducers and Applications, Springer, 2008.

[8] M. Link, "Solidly mounted ZnO shear mode film bulk acoustic resonators for sensing applications in liquids" in *IEEE Transactions on Ultrasonics Ferroelectrics and Frequency Control 53(2)*, 2006.

[9] M. DeMiguel-Ramos et al., "Gravimetric biosensor based on a 1.3 GHz AlN shear-mode solidly mounted resonator" *Sensors and Actuators B: Chemical,* vol. 239, pp. 1282-1288, 2017.

[10] M. DeMigue-Ramos et al., "Optimized tilted c-axis AlN films for improved operation of shear mode resonators" *Thin Solid Films,* vol. 590, pp. 219-223, 2015.

[11] F. Martin et al., "Shear mode coupling and tilted grain growth of AlN thin films in BAW resonators" *IEEE Transactions on Ultrasonics, Ferroelectrics, and Frequency Control,* vol. 53, no. 7, pp. 1339-1343, 2006.

[12] D. Ballantine, Acoustic Wave Sensors, Academic Press, 1996.

[13] J. Curie and P. Curie, "Développement par compression de l'électricité polaire dans les cristaux hémièdres à faces inclinées", *Bulletin de la Société Minérologique de France,* vol. 3, pp. 90-93, 1880.

[14] G. Lippman, "*Principe de la conservation de l'électricité*" *Phys. Theor. Appl.*, pp.381-394, 1881.

[15] J. Curie and P. Curie, "Contractions et dilatations produites par des tensions dans les cristaux hémièdres à faces inclinées" *Comptes Rendus ,* vol. 93, p. 1137–1140, 1881.

[16] J. F. Rosenbaum, Bulk acoustic wave theory and devices, Artech House, 1988.

[17] P.Muralt, "Stress Coupled Phenomena: Piezoelectric Effect" in *Encyclopedia of Materials: Science and Technology (Second Edition)*, 2001, pp. 8894-8897.

[18] Y. Q. Fu, "Advances in piezoelectric thin films for acoustic biosensors, acoustofluidics and lab-on-chip applications" in *Progress in Material Science*, 2017, pp. 31-91.

[19] E. Iborra et al., "*Piezoelectric properties and residual stress of sputtered AlN thin films for MEMS applications*" *Sensor Actuat,* vol. 115, 2004.

[20] G. Sauerbrey, " Verwendung von Schwingquarzen zur Wägung dünner Schichten und zur Mikrowägung", in *Zeitschrift für Physik* vol 155, pp. 206–222,1959.

[21] M. DeMiguel Ramos, "High sensitivity biosensor based on shear mode AlN resonators for in liquid operation" Universidad Politecnica de Madrid, 2015.

[22] D. David, A. Feld et al. "After 60 years: A new formula for computing quality factor is warranted" in *IEEE Ultrasonics Symposium*, Beijing, China, 2008.

[23] G. Carlotti, "Elastic Characterization of Transparent and Opaque Films, Multilayers and Acoustic Resonators by Surface Brillouin Scattering: A Review" *Applied Science,* vol. 8, 2008.

[24] S. Jose et al., "Optimized Reflector Stacks for Solidly Mounted Bulk Acoustic Wave Resonators" *IEEE Transactions on Ultrasonics, Ferroelectrics, and Frequency Control,,* vol. 57, no. 12, 2010.

[25] S. Jose et al., "Acoustic dispersion of solidly mounted resonator with an optimized reflector stack for dual wave reflection".in *Proceedings of the IEEE International Ultrasonics Symposium. pp 91-94, 2010*

[26] X. Juan et al., "Fabrication and Frequency Response Characteristics of AlN-Based Solidly Mounted Resonator" *Chinese Physics Letters,* vol. 26, no. 4, 2009.

[27] N. Tanskaya et al., "The influence of surface roughness of Bragg reflector layers on characteristics of microwave solidly mounted resonator" in *International Siberian Conference on Control and Communications (SIBCON)*, 2015.

[28] K. Hashimoto, Surface Acoustic Wave Devices in Telecommunications, Springer, 2000.

[29] M. DeMiguel Ramos et al., "Influence of the electrical extensions in AlN-BAW resonators for in-liquid biosensors" *2014 European Frequency and Time Forum (EFTF),* pp. 301-304, 2014.

[30] T. Mirea, *THIN FILM ELECTROACOUSTIC RESONATORS FOR PHYSICAL AND CHEMICAL SENSING,* Universidad politecnica de Madrid, 2017.

[31] W. P. Mason, Physical Acoustics Principles and Method Academic Press vol.1A, Academic press, 1964.

[32] K. M. Lakin, "Modeling of thin film resonators and filters," in *IEEE Microwave Symposium Digest pp. 149–152.*, 1992.

[33] M. Lakin et al., "High-Q microwave acoustic resonators and filters" *IEEE Transactions on Microwave Theory and Techniques,* vol. 41, pp. 2139-2146, 1993.

[34] S. Jose, Reflector stack optimization for bulk acoustic wave resonator, University of Twente, 2011.

[35] M. DeMiguel-Ramos et al., "Induced surface roughness to promote the growth of tilted-AlN films for shear mode resonators" in *Joint European Frequency and Time Forum & International Frequency Control Symposium, 274-277*, 2013.

[36] J. Rosenbaum, Bulk Acoustic Wave Theory and Devices, 1988: Artech House AcousticsLibrary.

[37] T. Mirea et al., "Impact of FBAR design on its sensitivity as in-liquid gravimetric sensor" *Sensors and Actuators A: Physical,* vol. 289, pp. 87-93, 2019.

[38] E. Milyutin, "Theoretical and Experimental Study of Piezoelectric Modulated AlN Thin Films for Shear Mode BAW Resonators" École polytechnique fédérale de Lausanne, 2011.

[39] S. Upasham e. al., "Cardiac troponin biosensors: where are we now?," *Advanced Health Care Technologies,* vol. 4, pp. 1-13, 2018.